
Article:
Ahmed, A.A. and Susmel, L. orcid.org/0000-0001-7753-9176 (2018) Static assessment of plain/notched polylactide (PLA) 3D-printed with different in-fill levels: equivalent homogenised material concept and Theory of Critical Distances. Fatigue & Fracture of Engineering Materials and Structures. ISSN 8756-758X

https://doi.org/10.1111/ffe.12958

Static assessment of plain/notched polylactide (PLA) 3D-printed with different in-fill levels: equivalent homogenised material concept and Theory of Critical Distances

Adnan A. Ahmed, Luca Susmel
Department of Civil and Structural Engineering, the University of Sheffield,
Mappin Street, Sheffield S1 3JD, UK

Corresponding Author: Prof. **Luca Susmel**
Department of Civil and Structural Engineering
The University of Sheffield, Mappin Street, Sheffield, S1 3JD, UK
Telephone: +44 (0) 114 222 5073
Fax: +44 (0) 114 222 5700
E-mail: l.susmel@sheffield.ac.uk

ABSTRACT
In the present paper a novel approach based on the equivalent homogenised material concept and the Theory of Critical Distances is formulated to perform static assessment of plain/notched objects of polylactide (PLA) when this polymer is additively manufactured with different infill levels. The key idea is that the internal net structure resulting from the 3D-printing process can be modelled by keeping treating the material as linear-elastic, continuum, homogenous and isotropic, with the effect of the internal voids being taken into account in terms of change in mechanical/strength properties. This idea is initially used to assess the detrimental effect of the manufacturing voids on the static strength of the plain (i.e., un-notched) material. This is done by addressing this problem in a Kitagawa-Takahashi setting via the Theory of Critical Distances. Subsequently, this approach is extended to the static assessment of notched components of 3D-printed PLA, i.e., it is used to take into account simultaneously the effect of both manufacturing voids and macroscopic geometrical features. The accuracy and reliability of this design methodology was checked against a large number of experimental data generated by testing, under axial loading, plain specimens as well as notched samples (including open notches) of PLA. These specimens were manufactured by making the infill level vary in the rage 10%-90%. This validation exercise allowed us to demonstrate that the proposed approach is highly accurate, returning estimates falling within an error interval of ±20%. This remarkable level of accuracy strongly supports the idea that static assessment of 3D-printed materials with complex geometries and manufactured with different infill levels can be performed by simply post-processing conventional linear-elastic Finite Element (FE) solid models, i.e., without the need for modelling explicitly the detrimental effect of the manufacturing voids.

Keywords: Polylactide (PLA), additive manufacturing, homogenised equivalent material, critical distance.

Nomenclature

a	crack-length (or semi-crack length)
d_V	effective size of the manufacturing voids
r_n	notch root radius
t	thickness
w_g	gross width
w_n	net width
E	Young's modulus
F	axial force
L	Critical distance value calculated according to the TCD
K_{Ic}	Plane strain fracture toughness

Oxyz	System of coordinates
Oθr	Polar coordinates
ε_{exp}	experimental strain measured using the 50 mm gauge length extensometer
$\sigma_{0.2\%}$	0.2% proof stress
σ_{eff}	effective stress calculated according to the TCD
σ_g	gross nominal stress
σ_f	failure stress
σ_{fs}	fictitious stress in the plain specimens, i.e.: $\sigma_{fs} = F/(t \cdot w_n)$
$\sigma_{net,f}$	nominal net failure stress
σ_x, σ_y, τ_{xy}	normal and shear stresses
σ_{UTS}	ultimate tensile strength
θ_p	manufacturing angle

1. Introduction

Additive manufacturing (AM) technologies will underpin a new industrial revolution by allowing intricate and complex objects to be manufactured from virtual models via constant deposition of material layers. Owing to its specific and unique features, AM is then expected to lead to novel design paradigms resulting in structural components not only showing superior in-service mechanical performance, but also fabricated by diminishing usage of materials and energy. In this context, AM could also give rise to different and quicker solutions to repair damaged components, to fabricate parts remotely, and to make on-demand bespoke objects. In this setting, examination of the state of the art shows that the technologies that are already available in the market allow polymers, metallic materials, concrete, and composite materials to be 3D-printed effectively and at a relatively low cost.

In order to fully exploit the tremendous potential of AM, engineers must be able not only to model correctly the mechanical behaviour of additively manufactured (AM) structural components, but also to perform static assessment effectively. This explains the reason why in recent years a few investigations have been carried out to devise new design techniques specifically formulated to assess strength of 3D-printed components.

Thanks to the systematic R&D work that has been done since the beginning of the 1980s, certainly, the AM technologies that have reached the highest level of maturity are those optimised to 3D-print polymers, with acrylonitrile butadiene styrene (ABS) and polylactide (PLA) being the most commonly used materials.

PLA is a biodegradable linear thermoplastic aliphatic polyester that is manufactured from renewable sources such as corn starch or sugarcane. Owing to its physical properties, PLA can be manufactured very effectively and at low cost by using commercial 3D-printers making use of the so-called Fused Deposition Modelling (FDM) technology. The FDM AM process employs a heated nozzle which melts filaments of PLA that are unwound from a coil. By depositing the material being extruded via the nozzle directly onto the build plate, a layer of material is manufactured, with the horizontal motion of the nozzle allowing the specific shape of the layer being fabricated to be obtained accurately. As the extruded filaments are being deposited, they cool down and harden so that they bind to each other as well to the previously manufactured layer of material. When a layer is finished, the build plate lowers so that the deposition of the subsequent layer can start. In order to reach a higher level of superficial finishing, before fabricating a layer, 3D-printers manufacture the so-called “shell”, i.e., a perimetric wall that retains and delimit the material being deposited internally. The thickness of the shell is always recommended to be set equal to a multiple of the nozzle diameter, so that the formation of manufacturing defects is limited effectively. The presence of the shell also allows the density of the bulk material to be reduced, with this leading to objects that have a net-like internal structure. This is clearly an

important feature, because changing the infill level allows the weight of 3D-printed objects as well as the usage of material to be reduced markedly.
As far as AM PLA is concerned, examination of the state of the art demonstrates that, so far, the scientific community has focussed their attention on components 3D-printed by setting the infill level equal to 100%. Mechanical behaviour and static/fatigue strength of 100% infill AM PLA are influenced by different technological parameters that include [1-9]: layer thickness, nozzle size, manufacturing orientation, filling rate, feed rate, manufacturing rate, and filling temperature. In this context, it is interesting to observe that much experimental evidence suggests that, as long as objects are 3D-printed flat on the built plate, the effect of the raster orientation can be neglected with little loss of accuracy [6]. Further, the stress-strain behaviour of AM PLA is seen to be predominantly linear up to final breakage, with the level of ductility changing as the manufacturing direction changes [4, 6].
By making use of the equivalent homogenised material concept and the Theory of Critical Distances (TCD), the present paper aims to formulate and experimentally validate a novel approach suitable for performing static assessment of plain/notched components of AM PLA fabricated with infill levels lower than 100%.

2. TCD and Kitagawa–Takahashi's diagram under static loading

The TCD is the name which has been given by David Taylor [10] to a group of theories that use a material length scale parameter to estimate strength of components containing not only cracks, but also short, sharp and blunt notches. One of the key features of the TCD is that static assessment is performed by directly post-processing the linear-elastic stress fields in the vicinity of the assumed crack initiation locations [11-14]. This aspect results in a great simplification of the stress analysis problem, since the TCD allows real components to be designed without carrying out complex and time-consuming non-linear analyses [10, 12, 14].
The TCD takes as a starting point the hypothesis that static strength in the presence of geometrical features of all kinds can be estimated accurately via an effective stress, σ_{eff}, that is representative of the entire linear-elastic stress field acting on the material in a specific finite size region [10]. In this setting, this process zone can be thought of as that portion of material controlling the overall static strength of the component being designed. The size of the process zone is seen to depend on material microstructural features, local micro-mechanical properties, and characteristics of the physical mechanisms leading to final breakage [15].
According to this theoretical framework, a cracked/notched brittle material (100% infill AM PLA included [6]) subjected to static loading is assumed to fail as soon as σ_{eff} becomes equal to the material ultimate tensile strength [10].
The TCD effective stress can be determined according to different strategies, with this being done by simply defining a convenient material length scale parameter and a suitable integration domain.
Irrespective of the assumption being made to derive σ_{eff}, the TCD's critical distance is determined according to the following well-known definition [10, 16]:

$$L = \frac{1}{\pi}\left(\frac{K_{Ic}}{\sigma_{UTS}}\right)^2, \quad (1)$$

where K_{Ic} is the plane strain fracture toughness and σ_{UTS} is the ultimate tensile strength. Since length L depends on two material properties, it is in turn a material property which is different for different materials [10].
By changing size and shape of the integration domain used to calculate σ_{eff}, the TCD can be formalised according to either the Point Method (PM), the Line Method (LM), or the Area Method, i.e. (see also Figs 1a to 1d) [10]:

$$\sigma_{eff} = \sigma_y\left(\theta = 0, r = \frac{L}{2}\right) \text{ - Point Method (Fig. 1b)} \quad (2)$$

$$\sigma_{eff} = \frac{1}{2L}\int_0^{2L} \sigma_y(\theta = 0, r)\, dr \text{ - Line Method (Fig. 1c)} \quad (3)$$

$\sigma_{eff} = \frac{4}{\pi L^2}\int_0^{\frac{\pi}{2}}\int_0^{L}\sigma_1(\theta,r)\cdot r\cdot dr\cdot d\theta$ - Area Method (Fig. 1d) (4)

It can be noticed here that there is also a three-dimensional formulation of the TCD, which is known as the Volume Method [10]. According to this formalisation of the critical distance concept, σ_{eff} is calculated by averaging the linear-elastic maximum principal stress over a hemisphere centred at the tip of the stress raiser being assessed and having radius equal to 1.54L [17].

It is important to point out here that the linear-elastic TCD as reviewed in the present section is seen to be successful in estimating the static strength of notched components made not only from brittle [10, 11], but also from ductile materials [10, 12-15]. This is a consequence of the fact that, by its nature, the TCD can directly accommodate any material non-linearities into a linear-elastic constitutive law, with this being done by simply changing the way the adopted reference strength is defined [10, 12, 14]. In particular, when the mechanical behaviour of the material under investigation is predominantly brittle, the TCD inherent material strength can be taken directly equal to σ_{UTS} – this is the case for 3D-printed PLA [6]. In contrast, when the mechanical behaviour of the material being assessed is characterised by a non-linear stress-strain response, the TCD inherent strength becomes larger than σ_{UTS} and it must be determined by running appropriate experiments [10].

Although Eqs (2) to (4) can be used to design components containing geometrical features of all kinds, they can be derived rigorously solely for the case of an infinite plate containing a through-thickness central crack [18].

As far as cracked plates loaded in tension are concerned, another important aspect is that the TCD is capable of describing the transition from the short-crack to the long-crack regime [10, 19-21]. In particular, by using the classic analytical solution due to Westergaard [22] to describe the stress distribution in the vicinity of the crack tip, the PM and the LM can be expressed as followed, respectively [10]:

$\sigma_f = \sigma_{UTS}\sqrt{1-\left(\frac{a}{a+\frac{L}{2}}\right)^2}$ - Point Method (5)

$\sigma_f = \sigma_{UTS}\sqrt{\frac{L}{a+L}}$ - Line Method (6)

where σ_f is the nominal gross stress resulting in the breakage of the cracked plate and a is the semi-crack length.

The normalised Kitagawa–Takahashi diagram reported in Fig. 1e confirms that Eqs (5) and (6) are capable of correctly describing the transition from the short- to the long-crack regime. In particular, this diagram makes it evident that the PM and the LM return the same results for the extreme cases given by the two straight asymptotic lines, i.e. for the un-cracked material case (σ_{UTS}) and the long-crack case – with the latter being modelled according to Linear Elastic Fracture Mechanics (LEFM). As far as the transition region between short- and long-cracks is concerned, a direct comparison amongst these two different formalisations of the TCD shows that the LM is slightly more conservative than the PM (see Fig. 1e).

The theoretical framework summarised in the present section will be used in what follows to devise a novel methodology suitable for assessing static strength of plain and notched AM PLA fabricated by setting the infill level lower than 100%.

3. Manufacturing of the specimens, testing procedures, and experimental results

The specimens used in the present investigation were additively manufactured using 3D-printer Ultimaker 2 Extended+ together with 2.85mm diameter white filaments of New Verbatim PLA. The manufacturing parameter envelope being adopted was as follows: nozzle size equal to 0.4 mm, nozzle temperature to 240°C, build-plate temperature to 60°C, printing speed to 30 mm/s, layer height to 0.1 mm, and shell thickness to 0.4 mm.

The sketches reported in Fig. 2a show geometry and dimensions of the specimens that were tested under a displacement rate equal to 2mm/minute by using a Shimadzu universal axial machine. Local strains in the plain samples were gathered and measured via an extensometer having gauge length equal to 50 mm. Three samples were tested for any geometry/manufacturing configuration being investigated and all the tests were run up to complete breakage.
The results from all the experimental trials that were run according to the protocols described in this section are summarised in Tabs 1 to 3, with the meaning of the used symbols being explained in the Nomenclature.
As per Fig. 2a, we manufactured and tested notches with opening angle equal to 0° as well as to 135°. Since in continuum, homogenous, and isotropic materials the opening angle affects the gradients of the local linear-elastic stress field distributions [23], this was done to check in a more effective and rigorous way the overall accuracy of the methodology being proposed.
The specimens shown in Fig. 2a were all fabricated flat on the build-plate, with manufacturing angle θ_p being set equal to 0°, 30°, and 45°. As per Fig. 2b, angle θ_p was defined as the angle between printing direction y_p and the longitudinal axis of the samples themselves. Since the 3D-printer we used works by depositing the filaments always at ±45° to direction y_p (see Fig. 2b), changing the value of angle θ_p allowed us to vary effectively the raster orientation with respect to the direction along which the axial loading was applied during testing.
The un-notched specimens were manufactured by making the in-fill level vary in the range 10%-90%. The notched samples instead were fabricated with fill density equal to 30%, 50%, and 70%. Fig. 3a shows some examples of the net-like internal structure that was obtained in the plain specimens for different values of the fill density. For an in-fill level equal to 70%, Fig. 3a also shows how the effective size, d_V, of the manufacturing voids was defined, with d_V being measured - both in the plain and in the notched specimens – by using an optical microscope. The average values for the size, d_V, of the manufacturing voids are listed in Tabs 1 to 3.
As to the specimens being manufactured by setting the in-fill density lower than 100%, it is important to point out that the thickness of both the shell and the internal walls forming the net-like structure was equal to about 0.4 mm, i.e., approximately equal to the diameter of the nozzle.
The matrix of failures reported in Fig. 3b shows three examples of the cracking behaviour that was observed in the tested specimens of AM PLA. Irrespective of overall macroscopic geometry, manufacturing angle θ_p, and in-fill level, initiation as well as initial propagation of cracks in the shells were seen to occur always on planes that were almost perpendicular to the direction of the applied tensile force. This initial phase resulting in embryonic cracks having length of the order of 0.4 mm led to a subsequent propagation process occurring along paths that followed the directions of the internal walls forming the net-like structure of the samples (Fig. 3b). The observed cracking behaviour indicates that cracks propagated as a result of two prevailing failure mechanisms, i.e., de-bonding between adjacent layers and rectilinear cracking of the filaments forming the internal walls.
The graphs reported in Figs 4a and 5 show some examples of the force-displacement behaviour displayed by the plain and notched specimens being tested. In particular, the curves plotted in Figs 4a and 5 are those from the first test that was run for any geometry/manufacturing configuration being investigated.
The charts of Fig. 4a suggest that the plain samples were characterised by a force-displacement response that was almost linear up to the maximum force recorded during testing. If attention is focused on the non-linear part of the total deformation, the force-displacement graphs reported in Fig. 4a show that those samples fabricated by setting angle θ_p equal to 0° displayed a large level of tensile ductility resulting in an almost horizontal plateau. In contrast, in the specimens manufactured by setting θ_p equal to 30° and 45°, breakage took place as soon as the applied force reached its maximum value. Another important aspect that must be pointed out here is that the specimens never necked before breakage took place, with this holding true independently of the value of angle θ_p.

Turning to the force-displacement response displayed by the notched samples, the charts reported in Fig. 5 show that the curves being generated were all characterised by an initial branch that was predominantly linear, with this being followed by a branch that was markedly non-linear. To conclude, it can be noticed that, similar to what we observed in the plain specimens, the notched samples showing the largest degree of non-linearity were always those manufactured by setting angle θ_p equal to 0°.

4. Mechanical behaviour in terms of equivalent homogenised material

In a related research project [6], recently we tested a large number of plain and notched specimens fabricated by using the same parent material, the same 3D-printer, and the same manufacturing parameter envelope as the ones employed to fabricate the specimens considered in this article. The key difference between the previous and the present experimental campaign is that the results reported in Ref. [6] were all generated by testing samples 3D-printed by setting the fill density invariably equal to 100%.

One of the most relevant findings from our previous investigation was that, for specimens 3D-printed horizontally on the build-plate, the effect of the manufacturing direction could be disregarded, with this resulting just in a little loss of accuracy. In particular, all the experimental results used to determine the mechanical properties of the 100% in-fill AM PLA being tested were seen to fall within 2 standard deviations of the mean, with the obtained average values being as follows [6]: E=3479 MPa, $\sigma_{0.2\%}$=41.7 MPa, σ_{UTS}=42.9 MPa, and K_{Ic}=3.7 MPa·m$^{1/2}$.

As to the obtained value for K_{Ic}, it is important to recall here that the propagation of the cracks in the C(T) samples being tested was seen to be influenced by the orientation of the deposited filaments [6] - with this holding true even though all the fracture toughness values were within two standard deviations of the mean. In more detail, in the specimens manufactured by setting θ_p equal to 0° and 30°, the cracking behaviour was governed by mixed-mode fracture mechanisms. In contrast, in the samples with θ_p =45° the crack growth process was governed by a conventional pure Mode I propagation mechanism. Another important aspect is that K_{Ic} was determined without introducing any pre-cracks in the specimens. This was done so that the fracture toughness of the AM polymer being tested could be quantified by effectively taking into account the effect of the shell thickness as well [6].

As mentioned earlier, this paper summarises an attempt of devising an alternative TCD-based design methodology suitable for performing static assessment of AM PLA when this material is 3D-printed by adopting a fill density lower than 100%. As it will be discussed below in detail, this novel formalisation of the TCD is based on the idea that mechanical behaviour and strength of PLA additively manufactured with in-fill levels lower that 100% can be modelled by simply using an equivalent material which is linear-elastic, continuum, homogeneous and isotropic. By bearing in mind this initial hypothesis, the force vs. displacement curves obtained from the plain specimens were then re-analysed in terms of fictitious stress, σ_{fs}, and experimental strain, ε_{exp} (i.e., the strain measured by using the 50 mm gauge length extensometer). In more detail, σ_{fs} was calculated by simply diving the force applied during testing, F, by the cross-sectional area determined by neglecting the presence of the manufacturing voids, i.e.:

$$\sigma_{fs} = \frac{F}{t \cdot w_n}, \tag{7}$$

where t is the thickness and w_n the net width of the gauge length region.

As an example, the σ_{fs} vs. ε_{exp} diagrams reported in Fig. 4b show the curves that were obtained by post-processing according to this simple procedure the force-displacement data displayed in Fig. 4a. In agreement with what was observed in other related investigations (see, for instance, Refs [2, 4, 6] and the references reported therein), the σ_{fs} vs. ε_{exp} diagrams of Fig. 4a strongly support the idea that the stress vs. strain behaviour of the tested AM material could be treated as purely linear-elastic up to the maximum stress recorded during testing, with this assumption resulting just in a little loss of accuracy. As to the non-linear part of the total deformation instead, according

to the charts of Fig. 4b, the specimens with θ_p equal to 0° were seen to be characterised by a large level of tensile ductility. In contrast, the samples manufactured by setting θ_p equal to 30° and 45° were seen to fail as soon as the applied fictitious stress reached its maximum value.
Similar to what is seen in Fig. 4b, the σ_{fs} vs. ε_{exp} curves obtained from the experiments run by testing the plain specimens (Tab. 1) were all characterised by the same type of profile as the one which is usually displayed by conventional materials when the problem is addressed using standard engineering stresses and strains. Therefore, the results summarised in Tab. 1 were systematically re-analysed in terms of fictitious stress, σ_{fs}, and experimental strain, ε_{exp}, to determine the failure strength σ_f (i.e., the maximum value of the fictitious stress recorded during testing), the 0.2% fictitious proof stress, $\sigma_{0.2\%}$, and the fictitious elastic modulus, E.
The results obtained by re-analysing the results listed in Tab. 1 according to this *modus operandi* are summarised in the charts of Figs 6a, 6b, and 6c. For the sake of completeness, in these diagrams we reported also the results that we obtained by testing 100% in-fill plain specimens [6]. As to the latter set of results, it is interesting to observe that in the absence of manufacturing voids the use of definition (7) returns nothing but the conventional engineering stress.
As expected, the diagrams of Figs 6a to 6c confirm that σ_f, $\sigma_{0.2\%}$, and E decrease as the fill density decreases. Another important aspect is that, as per the 100% in-fill case, the values of the fictitious mechanical properties are seen not to be affected by manufacturing angle θ_p.
By carefully observing the charts of Figs 6a, 6b, and 6c, it is possible to see that the values of σ_f, $\sigma_{0.2\%}$, and E drop quite markedly moving from the 100% down to the 90% in-fill case. This can be explained by considering the specific feature of the meso-structure of AM PLA. In particular, for the 100% in-fill case, the overall mechanical behaviour depends on three aspects, i.e.: (i) the mechanical properties of the deposition filaments, (ii) the forces bonding together the filaments belonging to the same layer and, finally, (iii) the forces bonding together adjacent layers. These three aspects result in the fact that in AM PLA manufactured by setting the fill density equal to 100% the cracking behaviour is governed by three distinct mechanisms, i.e.: (i) rectilinear cracking of the filaments and de-bonding occurring (ii) between adjacent filaments as well as (iii) between adjacent layers [6]. In contrast, when the infill level is lower than 100%, the forces bonding together the filaments belonging to the same layer disappear, with this having a detrimental effect on the overall mechanical properties of AM PLA. This explains why the mechanical properties for the 90% in-fill case are markedly lower than the corresponding ones characterising the material manufactured by setting the fill density equal to 100%, with this holding true even if the manufacturing internal voids were very small in the 90% in-fill specimens.
The considerations reported in the present section strongly support the idea that, independently of fill density, AM PLA can be modelled effectively by simply using an equivalent material that is continuum, homogenous and isotropic. This lays the foundations for the theoretical framework that will be discussed and validated in the next sections.

5. Modelling plain static strength of AM PLA with different infill levels

According to the diagram of Fig. 6a, as expected, the fictitious failure strength, σ_f, increases as the fill density increases. Therefore, the first step in the theoretical development of the novel approach being proposed in the present paper is devising a strategy suitable for estimating static strength of plain AM PLA as the size of the internal manufacturing voids varies.
Consider the uniaxially loaded plain strip of AM PLA that is sketched in Fig. 7a. This strip is assumed to be 3D-printed by setting the fill density lower than 100%, with this resulting in an equivalent size of the internal voids equal to d_V (Fig. 7a). This plain strip is hypothesised to be in the incipient failure condition so that the applied fictitious stress is equal to σ_f.
Consider now an infinite plate (Fig. 7b) of a continuum, homogeneous, isotropic, linear-elastic material having σ_{UTS} and K_{Ic} equal to the corresponding values that can be determined experimentally by testing 100% in-fill specimens of the same AM material as the one the strip

sketched in Fig. 7a is made of. The infinite plate of Fig. 7b is also supposed to contain a central through-thickness crack having semi-length equal to a_{eq}. The length of the crack is set so that the plate of Fig. 7b fails when the applied gross remote stress becomes equal to the fictitious failure stress, σ_f, that would result in the breakage of the AM plain strip of Fig. 7a. Therefore, also the plate with a central through-thickness crack of Fig. 7b is assumed to be in the incipient failure condition. Another important aspect is that, since the specimen of Fig. 7b is schematised as an infinite plate containing a through-thickness central crack, the corresponding LEFM shape factor is invariably equal to unity, with this holding true independently of the crack's semi-length, a_{eq}.
According to the hypotheses being formed, LEFM postulates that the cracked plate of Fig. 7b fails as soon as the resulting stress intensity factor becomes equal to the material fracture toughness. Accordingly, the failure condition for the homogenised equivalent cracked material can be expressed as follows:

$$K_{Ic} = \sigma_f \sqrt{\pi \cdot a_{eq}}, \tag{8}$$

where equality (8) is valid provided that the plate of Fig. 7b is weakened by a long-crack. If this is the case, then Eq. (8) can directly be used to estimate a_{eq}, i.e.:

$$a_{eq} = \frac{1}{\pi}\left(\frac{K_{Ic}}{\sigma_f}\right)^2 \tag{9}$$

The next step in the reasoning is then assuming that there is a univocal link between the semi-length of the crack in the plate of Fig. 7b and the size of the manufacturing voids in the plain strip of Fig. 7a. Correspondingly, it is possible to write:

$$a_{eq} = f(d_V), \tag{10}$$

where $f(d_V)$ is a transformation function turning the 3D-printed plain strip under investigation (Fig. 7a) into an equivalent continuum, homogeneous, isotropic, linear-elastic, cracked material (Fig. 7b).
The fundamental idea behind this transformation process is that the equivalence between the two situations depicted in Fig. 7 is assured by imposing that both the AM strip and the cracked plate fail as soon as the applied stress becomes equal to σ_f. This idea works provided that: (i) for the AM strip the stress is defined according to Eq. (7) – i.e., by neglecting the presence of the net-like voids, and (ii) for the cracked plate the stress is calculated by referring to the gross area – i.e., by neglecting the presence of the crack.
As mentioned earlier, Eq. (9) can be used to estimate a_{eq} as long as the size of the AM voids being considered results, via function (10), in an equivalent homogenised material that is weakened by a long crack. However, since it is reasonable to believe that manufacturing voids behave more and more like short-cracks as the fill density approaches 100%, clearly Eq. (9) does not represent a solution of general validity. This intrinsic limitation of LEFM can be overcome by using the TCD. As reviewed in Section 2, one of the key features of the TCD is that this theory is capable of modelling the transition from the short- to the long-crack regime (see Fig. 1e). Further, for the case of an infinite plate containing a central through-thickness crack, the PM and LM allow the transition between these two regimes to be modelled directly via closed form equations – i.e., Eq. (5) and Eq. (6), respectively. Therefore, thanks to its unique features, the TCD is the best tool that should be used to model in a more general way the transformation process sketched in Fig. 7.
Consider then the PM formalised to assess the case of a through-thickness crack in an infinite plate loaded in tension – see Eq. (5). If the generic semi-crack length is replaced with the equivalent semi-crack length, it is straightforward to solve Eq. (5) for a_{eq}, obtaining:

$$a_{eq} = f(d_V) = \frac{L}{2\sigma_f^2}\left\{\left(\sigma_{UTS}^2 - \sigma_f^2\right) + \sqrt{\left(\sigma_f^2 - \sigma_{UTS}^2\right)^2 - \sigma_f^2\left(\sigma_f^2 - \sigma_{UTS}^2\right)}\right\} \tag{11}$$

In a similar way, by using the LM in the form of Eq. (6), the equivalent semi-crack length takes on the following value:

$$a_{eq} = f(d_V) = L\left[\left(\frac{\sigma_{UTS}}{\sigma_f}\right)^2 - 1\right] \tag{12}$$

As stated above, the constants that quantify the static strength of the equivalent homogenised cracked material used in the transformation process of Fig. 7 are assumed to be equal to the corresponding strength properties that are determined experimentally from 100% in-fill specimens made of the AM material under investigation. Therefore, σ_{UTS} and K_{Ic} associated with the 100% in-fill AM material being designed are to be used to estimate, as per definition (1), the critical distance value, L, that is needed to calculated a_{eq} via Eqs (11) and (12).
The last step in the reasoning is defining transformation function $f(d_V)$ so that it can be calibrated properly. Ideally, this process should be optimised so that the experimental effort being required to calibrate function $f(d_V)$ is minimised. To this end, the hypothesis can be formed that the link between a_{eq} and d_V is given by a simple linear relationship, i.e.:

$$a_{eq} = f(d_V) = k_t \cdot d_V \tag{13}$$

where k_t is a dimensionless transformation constant. The key advantage of using a simple linear function is that, for a given value of d_V, constant k_t in Eq. (13) can be determined either via Eq. (11) as:

$$k_t = \frac{a_{eq}}{d_V} = \frac{L}{2 \cdot d_V \cdot \sigma_f^2}\left\{\left(\sigma_{UTS}^2 - \sigma_f^2\right) + \sqrt{\left(\sigma_f^2 - \sigma_{UTS}^2\right)^2 - \sigma_f^2\left(\sigma_f^2 - \sigma_{UTS}^2\right)}\right\} \tag{14}$$

or via Eq. (12) as:

$$k_t = \frac{a_{eq}}{d_V} = \frac{L}{d_V}\left[\left(\frac{\sigma_{UTS}}{\sigma_f}\right)^2 - 1\right] \tag{15}$$

In Eqs (14) and (15) σ_{UTS} is the static strength of the AM material for a fill density equal to 100%, whereas σ_f is the fictitious failure stress experimentally determined for the size, d_V, of the manufacturing voids used for calibration.
As soon as transformation function $f(d_V)$ is calibrated, the PM and the LM can directly be used to estimate the failure strength of the AM PLA under investigation for any in-fill level. This can be done by simply rewriting Eqs (5) and (6) as follows:

$$\sigma_f = \sigma_{UTS}\sqrt{1 - \left(\frac{a_{eq}}{a_{eq}+\frac{L}{2}}\right)^2} = \sigma_{UTS}\sqrt{1 - \left[\frac{f(d_V)}{f(d_V)+\frac{L}{2}}\right]^2} = \sigma_{UTS}\sqrt{1 - \left(\frac{k_t \cdot d_V}{k_t \cdot d_V+\frac{L}{2}}\right)^2} \text{ - Point Method} \tag{16}$$

$$\sigma_f = \sigma_{UTS}\sqrt{\frac{L}{a_{eq}+L}} = \sigma_{UTS}\sqrt{\frac{L}{f(d_V)+L}} = \sigma_{UTS}\sqrt{\frac{L}{k_t \cdot d_V+L}} \text{ - Line Method} \tag{17}$$

In order to check the accuracy and reliability of the approach formulated in the present section, Eqs (16) and (17) were used to estimate the static strength of the plain specimens being tested (see Tab. 1). In more detail, initially, the material ultimate tensile strength (σ_{UTS}=42.9 MPa) and the fracture toughness (K_{Ic}=3.7 MPa·m$^{1/2}$) experimentally determined [6] by testing specimens of AM PLA 3D-printed by setting the in-fill level equal to 100% were used together with Eq. (1) to determine critical distance L, obtaining L=2.4 mm.
Subsequently, the results from the plain specimens of PLA additively manufactured with an in-fill level equal to 80% (Tab. 1) were used to calibrate transformation function $f(d_V)$, Eq. (13). In particular, for any of the nine results obtained by setting the fill density equal to 80% and the manufacturing angle, θ_p, equal to 0°, 30°, and 45°, transformation constant k_t was determined according to the PM via Eq. (14) as well as according to the LM via Eq. (15). The nine values for the transformation constant being determined were subsequently averaged, with this process resulting in a k_t value equal to 35.5 for the PM and to 33.1 for the LM.
The two Kitagawa–Takahashi diagrams of Fig. 8 summarise the overall accuracy that was obtained by employing Eqs (16) and (17) to estimate the static strength of the plain specimens of AM PLA being tested.
These two charts make it evident that the use of the proposed approach results in a remarkable level of accuracy down to an in-fill level equal to 30%. In contrast, the estimates obtained for a fill density equal to 20% as well as to 10% clearly deviate from the predicted trend. This fact is not at all surprising since 3D-printed objects behave as lattice structures when the internal walls' mesh

becomes very course [24]. Accordingly, the use of the equivalent homogenised material concept to model mechanical behaviour and strength of objects 3D-printed with a very low fill density is no longer justified. This sets the lower limit for the usage of the proposed methodology in situations of practical interest.
It is important point out here that the same transformation process as the one summarised in Fig. 7 could have been formalised considering also other geometrical configurations for the equivalent homogenised cracked material (such as, for instance, a finite plate containing two lateral cracks). However, this *modus operandi* would increase the complexity of the solution unnecessarily, since the constitutive relationships being needed should be derived by incorporating into the transformation function also the shape factor. In contrast, using as reference configuration for the equivalent homogenised cracked material an infinite plate containing a central crack allows the problem to be formalised in a very simple and elegant way, with the shape factor being invariably equal to unity.
To conclude, it is important to highlight that the high level of accuracy reached by applying the approach being formulated in the present section was obtained by using a simple linear transformation law, Eq. (13). However, it is clear that other types of functions can be used to express $f(d_V)$, with this allowing our theoretical framework to be extended to the static assessment of other type of net-like/honeycomb-like materials (i.e., not only 3D-printed materials).

6. Assessing notch static strength of AM PLA with different infill levels

Thanks to its specific features, AM allows objects having complex forms to easily be fabricated by reaching a very high level of accuracy in terms of both shape and dimensions. However, the fact that 3D-printed components can contain very complex geometrical features results in very complex localised stress concentration phenomena that reduce markedly the overall strength of the components themselves. Therefore, structural engineers need simple and reliable design rules so that static assessment of 3D-printed materials can be performed accurately. To this end, in this section the combined use of the TCD and the equivalent homogenised material concept is extended to the case of notched components made of AM PLA.
Consider the uniaxially-loaded notched objected sketched in Fig. 9a. This component is assumed to be additively manufactured by setting the in-fill level lower than 100%, with this resulting in internal voids having average size equal to d_V (Fig. 9a).
To consistently apply the TCD to estimate static strength, the notched AM object of Fig. 9a is modelled as a body that (i) has the same shape and dimensions as the object being designed and (ii) is made of a linear-elastic material which is continuum, homogenous, and isotropic (Fig. 9b). Having formed these initial hypotheses, the PM, LM, and Area Method are then applied by assuming that the size of the process zone does not change as the size of the voids varies. Accordingly, it is proposed that the required critical distance, L, is estimated directly via Eq. (1), where the values for σ_{UTS} and K_{Ic} being used are those experimentally determined from specimens 3D-printed by setting the in-fill level equal to 100% (Fig. 9b). In this setting, since, for a given AM material, length scale parameter L does not change, the detrimental effect of the manufacturing voids is proposed here to be taken into account by simply adjusting the material intrinsic static strength according either to Eq. (16) or to Eq. (17).
As per this *modus operandi*, owing to the fact that the AM component being designed is assumed to be made of a continuum, homogenous, isotropic, linear-elastic material, the fictitious local stress fields (Fig. 9c) used to calculate the effective stress according to the TCD can then be determined directly either by solving conventional FE models or by using available analytical solutions.
As soon as the fictitious local stress fields are known, effective stress σ_{eff} can then be calculated by applying the TCD in the form of either the PM, Eq. (2), the LM, Eq. (3), or the Area Method, Eq. (4). Owing to the fact that the AM material being designed is assumed to be weakened by the

presence of the manufacturing voids, the incipient failure condition can then be expressed as follows:

$$\sigma_{eff} = \sigma_f \tag{18}$$

where the intrinsic static strength of the material within the process zone, σ_f, is directly estimated according either to Eq. (16) or to Eq. (17). In particular, as far as the PM is concerned, by combining Eq. (2) with Eq. (16), failure condition (18) can directly be re-written as (Fig. 9c):

$$\sigma_{eff} = \sigma_y\left(\theta = 0, r = \frac{L}{2}\right) = \sigma_{UTS}\sqrt{1 - \left[\frac{f(d_V)}{f(d_V)+\frac{L}{2}}\right]^2} = \sigma_{UTS}\sqrt{1 - \left(\frac{k_t \cdot d_V}{k_t \cdot d_V + \frac{L}{2}}\right)^2} \tag{19}$$

In a similar way, combining Eq. (3) with Eq. (17) allows condition (18) to directly be expressed according to the LM as:

$$\sigma_{eff} = \frac{1}{2L}\int_0^{2L} \sigma_y(\theta = 0, r)\, dr = \sigma_{UTS}\sqrt{\frac{L}{f(d_V)+L}} = \sigma_{UTS}\sqrt{\frac{L}{k_t \cdot d_V + L}} \tag{20}$$

The accuracy and reliability of the novel reformulation of the TCD being proposed in the present section was checked against the experimental results we generated by testing the notched specimens shown in Fig. 2a (see also Tabs 2 and 3). To this end, initially, the linear-elastic stress fields needed to calculate the TCD effective stress were determined by post-processing the results from simple linear-elastic bi-dimensional models solved using FE code ANSYS®. The notched specimens being tested were modelled using bi-dimensional element Plane183, with the mapped mesh in the vicinity of the notch tips being gradually refined until convergence occurred. It is worth pointing out here that, as per the hypotheses being discussed in the present section, these FE analyses were run by modelling the material as a continuum, homogenous, isotropic, linear-elastic medium. This means that the relevant stress fields were determined without explicitly simulating the presence of the manufacturing voids.

A critical distance value of 2.4 mm was calculated via definition (1) by using the relevant material properties we determined by testing specimens manufactured with a fill density of 100%, i.e. σ_{UTS}=42.9 MPa and K_{Ic}=3.7 MPa·m$^{1/2}$ [6].

After estimating a value of 2.4 mm for critical distance L, the fictitious linear-elastic stress fields determined using FE code ANSYS® were post-processed to calculate, in the incipient failure condition, σ_{eff} according to the PM, Eq. (2), the LM, Eq. (3), and the Area Method, Eq. (4). The PM and the LM were then used in the form of Eq. (19) and Eq. (20), respectively, where, according to the charts of Fig. 8, transformation constant k_t was taken equal to 35.5 for the PM and to 33.1 for the LM.

In order to apply the Area Method, the corresponding effective stress, σ_{eff}, was determined by post-processing the numerical linear-elastic stress fields according to Eq. (4). Failure condition (18) was then expressed by calculating intrinsic static strength σ_f according to the PM, Eq. (16), with transformation constant k_t being taken equal to 35.5.

The error charts reported in Fig. 10 summarise the overall accuracy that was obtained by applying the new formalisation of the PM, LM, and Area Method proposed in the present section. In these diagrams, the error was calculated as follows:

$$Error = \frac{\sigma_{eff} - \sigma_f}{\sigma_f}\ [\%] \tag{21}$$

where an error larger than zero means that the estimates were conservative, whereas an error lower than zero means that the predictions were non-conservative.

As to the error charts of Fig. 10, it is important to point out that the experimental values being reported were calculated by averaging the three results from any geometry/manufacturing configuration being investigated (see also Tabs 2 and 3).

The diagrams shown in Figs 10a, 10b, and 10c make it evident that the TCD applied along with the equivalent homogenised material concept was successful in estimating the static strength of the U-notched specimens additively manufactured by setting the in-fill level lower than zero (Tab. 2). In particular, for this notch geometry, the systematic usage of the proposed design

methodology was seen to result in estimates falling mainly within an error interval of ±20%, with the Area Method (Fig. 10c) returning the largest level of conservatism.
As to the U-notched specimens being tested, it is important to highlight also that, according to the charts of Figs 6d, 6e, and 6f, their static strength was not at all affected by manufacturing angle θ_p. This explains why the predictions made by using the approach being proposed are seen to consistently fall within an error interval of ±20% (Figs 10a to 10c). In contrast, according to the charts of Fig. 6g, 6h, and 6i, the static strength of the specimens containing open notches was instead affected markedly by manufacturing angle θ_p (see also Tab. 3). In particular, the nominal net failure stress, $\sigma_{net,f}$, determined by testing the specimens manufactured by setting θ_p=45° was seen to be 25%-50% higher than the corresponding static strength experimentally determined by testing the samples with θ_p equal to 0° and to 30° (see also the force-displacement curves for the open notches reported in Fig. 5). By carefully inspecting the broken samples, it was straightforward to see that this apparent increase in static strength was simply a consequence of the way the 3D-printer being used fabricated these specimens: for θ_p=45° the internal walls were manufactured very close to the notch tips, with this resulting, in the crack initiation regions, in shells having thickness approaching 0.8 mm (i.e., approximately twice as thick as the corresponding shells in the specimens manufactured with θ_p equal to 0° and to 30°). This explains the reason why, according to the error charts reported in Fig. 10d to 10f, the use of the novel TCD-based approach being proposed returned very accurate predictions for open notches with θ_p equal to 0° and to 30°, with the estimates for the θ_p=45° cases being characterised by a certain level of conservatism.
However, owing to the complex micro/meso-structure characterising 3D-printed PLA, certainly, the level of accuracy shown in Fig. 10 is satisfactory. In particular, it is satisfactory also because, as far as conventional engineering materials are concerned, it is not possible to distinguish between an error of ±20% and an error of 0% due to the well-known physiological problems that are associated with testing as well as with numerical analyses/post-processing [10].
It is important to highlight here that the validation exercise discussed in the present section could have been done also by following a different (and much more “gentile”) strategy. In particular, rather than estimating the intrinsic static strength via Eqs (16) and (17), the experimental values for σ_f we determined by testing the un-notched specimens (see Tab. 1 and Figs 6a to 6c) could have been used directly in Eq. (18). Although, clearly, this would have been a reasonable validation methodology, we decided to check the accuracy of the approach being proposed by considering a scenario that was more realistic, i.e., intrinsically more demanding and challenging. In particular, since in situations of practical interest structural engineers are expected to have limited access to experimental resources, they cannot always test a large number of plain specimens manufactured by making the in-fill level vary systematically as we did in the present investigation. This means that, for a given in-fill level, they must be able to assess notch static strength by also estimating the necessary intrinsic static strength. Having in mind this important aspect, we then decided to validate the proposed approach by estimating σ_f via Eqs (16) and (17), with this allowing us to express a much more severe verdict about the accuracy and reliability of our novel design methodology.
To conclude, it can be observed that, in a way, the satisfactory degree of accuracy being obtained is not at all surprising, since the TCD was recently used successfully also to estimate the static strength of notched specimens made of polymeric cellular materials characterised by different levels of density [25, 26].

7. Conclusions

The present investigation aims to formulate a novel approach based on the combined use the equivalent homogenised material concept and the TCD suitable for performing static assessment of plain/notched objects of PLA additively manufactured with different infill levels.

The accuracy and reliability of the new approach being devised was checked against numerous experimental results generated by testing specimens of AM PLA containing different geometrical features (open notches included) and fabricated by changing not only the fill density, but also the manufacturing angle, θ_p.

According to the experimental results being generated and the validation exercise being performed, the key conclusions can be summarised as follows:

- independently of manufacturing angle θ_p and in-fill level, the mechanical behaviour of AM PLA can be model as linear-elastic up to final breakage, with this resulting just in a little loss of accuracy;
- the cracking behaviour of plain and notched objects of AM PLA is governed by the orientation of the internal walls;
- the static strength of plain and notched objects of AM PLA decreases as the size of the manufacturing voids increases;
- the TCD applied along with the equivalent homogenised material concept is seen to be successful in modelling the static strength of plain AM PLA as the size of the internal manufacturing voids increases;
- the TCD applied along with the equivalent homogenised material concept is seen to be successful in estimating notch static strength as the size of the internal manufacturing voids varies, with its use returning predictions that fall mainly within an error interval of ±20%;
- in terms of static assessment, the key advantage of the proposed approach is that the necessary stress fields can be determined from conventional FE models done by assuming that the material being designed is continuum, homogeneous, isotropic, and linear-elastic;
- the use of the equivalent homogenised material concept to model mechanical behaviour and strength of objects 3D-printed with a very low fill density is no longer justified when the internal walls' mesh becomes very course (i.e., when the objects under consideration behave like lattice structures);
- more works needs to be done in this area to extend the use of our theoretical framework to the static assessment of other type of net-like/honeycomb-like materials (i.e., not only 3D-printed materials).

References

[1] J.D. Ciurana, Selecting process parameters in RepRap additive manufacturing system for PLA scaffolds manufacture, Procedia CIRP 5 (2013) 152-157.

[2] A. Lanzotti, M. Grasso, G. Staiano, M. Martorelli, The impact of process parameters on mechanical properties of parts fabricated in PLA with an open-source 3-D printer, Rapid Prototyping J. 21 5 (2015) 604-617.

[3] J.M. Chacón, M.A. Caminero, E. García-Plaza, P.J. Núñez, Additive manufacturing of PLA structures using fused deposition modelling: Effect of process parameters on mechanical properties and their optimal selection, Mater. Des. 124 (2017) 143-157.

[4] Y. Song, Y. Li, W. Song, K. Yee, K.-Y. Lee, V.L. Tagarielli, Measurements of the mechanical response of unidirectional 3D-printed PLA, Mater. Des. 123 (2017) 154-164.

[5] C. Casavola, A. Cazzato, V. Moramarco, C. Pappalettere, Orthotropic mechanical properties of fused deposition modelling parts described by classical laminate theory, Mater. Des. 90 (2016) 453-458.

[6] A. A. Ahmed, L. Susmel, A material length scale–based methodology to assess static strength of notched additively manufactured polylactide (PLA). Fatigue Fract Eng Mater Struct. 41 (2018) 2071-2098.

[7] T. Letcher, M. Waytashek, Material property testing of 3D-printed specimen in PLA on an entry-level 3D-printer. In: Proceedings of the ASME 2014 International Mechanical Engineering

Congress & Exposition (IMECE2014), 14-20 November 2014, Montreal, Quebec, Canada, IMECE2014-39379.
[8] F. Afrose, S.H. Masood, P. Iovenitti, M. Nikzad, I. Sbarski, Effects of part build orientations on fatigue behaviour of FDM-processed PLA material. Prog. Addit. Manuf. 1 (2016) 21-28.
[9] O. H. Ezeh, L. Susmel, On the fatigue strength of 3D-printed polylactide (PLA). Procedia Structural Integrity 9 (2018) 29-36.
[10] D. Taylor, The Theory of Critical Distances: A new perspective in fracture mechanics. Elsevier, Oxford, UK 2007.
[11] L. Susmel, D. Taylor, The theory of critical distances to predict static strength of notched brittle components subjected to mixed-mode loading. Eng Frac Mech 75 (2008) 534-550.
[12] L. Susmel, D. Taylor, On the use of the Theory of Critical Distances to predict static failures in ductile metallic materials containing different geometrical features. Eng Fract Mech 75 (2008) 4410-4421.
[13] L. Susmel, D. Taylor, The Theory of Critical Distances to estimate the static strength of notched samples of Al6082 loaded in combined tension and torsion. Part I: Material cracking behaviour. Eng Fract Mech 77 (2010) 452–469.
[14] L. Susmel, D. Taylor, The Theory of Critical Distances to estimate the static strength of notched samples of Al6082 loaded in combined tension and torsion. Part II: Multiaxial static assessment. Eng Fract Mech 77 (2010) 470–478.
[15] A.A.H. Ameri, J.B. Davison, L. Susmel, On the use of linear-elastic local stresses to design load-carrying fillet-welded steel joints against static loading. Eng Fract Mech 136 (2015) 38-57.
[16] J.M. Whitney, R.J. Nuismer, Stress Fracture Criteria for Laminated Composites Containing Stress Concentrations. J Compos Mater 8 (1974) 253-65.
[17] D. Bellett, D. Taylor, S. Marco, E. Mazzeo, J. Guillois, T. Pircher, The fatigue behaviour of three-dimensional stress concentrations. Int J Fatigue 27 (2005) 207-221.
[18] D. Taylor, Geometrical effects in fatigue: a unifying theoretical model. Int J Fatigue 21 (1999) 413-420.
[19] D. Taylor, Predicting the fracture strength of ceramic materials using the theory of critical distances. Eng Fract Mech 71 (2004) 2407-2416.
[20] H. Askes, P. Livieri, L. Susmel, D. Taylor, R. Tovo, Intrinsic material length, Theory of Critical Distances and Gradient Mechanics: analogies and differences in processing linear-elastic crack tip stress fields. Fatigue Fract Engng Mater Struct. 36 (2013) 39-55.
[21] L. Susmel, H. Askes, T. Bennett, D. Taylor, Theory of Critical Distances vs. Gradient Mechanics in modelling the transition from the short- to long-crack regime at the fatigue limit. Fatigue Fract Engng Mater Struct. 36 (2013) 861-869.
[22] H.M. Westergaard, Bearing pressures and cracks. J Appl Mech A 61 (1939) 49-53.
[23] B. Atzori, P. Lazzarin, R. Tovo, Stress field parameter to predict the fatigue strength of notched components. J. Strain Anal. Eng. 34 (1999) 437-453.
[24] T. D. Ngo, A. Kashani, G. Imbalzano, K. T.Q. Nguyen, D. Hui, Additive manufacturing (3D printing): A review of materials, methods, applications and challenges. Composites Part B 143 (2018) 172–196.
[25] R. Negru, L. Marsavina, H. Filipescu, C. Căplescu, T. Voiconi, Assessment of brittle fracture for PUR materials using local strain energy density and theory of critical distances. Theor Appl Fract Mec 79 (2015) 62–69
[26] R. Negru, L. Marsavina, T. Voiconi, E. Linul, H. Filipescu, G. Belgiu, Application of TCD for brittle fracture of notched PUR materials. Theor Appl Fract Mec 80 (2015) 87–95.

Tables

Table 1 *(continued on the next two pages)*. Summary of the experimental results generated by testing the un-notched specimens.

Code	θ_P	In-fill	w_n	t	A_n	F_f	E	$\sigma_{0.2\%}$	σ_f	d_V
	[°]	*[%]*	*[mm]*	*[mm]*	*[mm^2]*	*[N]*	*[MPa]*	*[MPa]*	*[MPa]*	*[mm]*
P0_10_1	0	10	14.99	4.07	61.01	505	634	7.8	8.3	
P0_10_2	0	10	15.03	4.05	60.87	531	660	8.2	8.7	10.7
P0_10_3	0	10	15.05	4.05	60.95	529	692	8.2	8.7	
P0_20_1	0	20	14.98	4.00	59.92	561	725	8.6	9.4	
P0_20_2	0	20	14.92	3.95	58.93	538	709	8.4	9.1	4.98
P0_20_3	0	20	14.96	3.98	59.54	537	706	8.4	9.0	
P0_30_1	0	30	14.94	4.07	60.81	599	743	8.7	9.9	
P0_30_2	0	30	14.92	4.02	59.98	641	774	9.3	10.7	1.36
P0_30_3	0	30	14.99	4.02	60.26	638	773	9.4	10.6	
P0_40_1	0	40	15.02	4.00	60.08	721	867	10.2	12.0	
P0_40_2	0	40	15.00	4.08	61.20	723	857	9.7	11.8	0.88
P0_40_3	0	40	14.97	4.05	60.63	726	884	10.9	12.0	
P0_50_1	0	50	14.95	4.06	60.70	829	984	11.9	13.7	
P0_50_2	0	50	15.00	4.04	60.60	842	965	12.2	13.9	0.62
P0_50_3	0	50	15.03	4.07	61.17	816	950	11.0	13.3	
P0_60_1	0	60	15.10	4.05	61.16	971	1126	13.3	15.9	
P0_60_2	0	60	15.03	4.03	60.57	1004	1182	14.1	16.6	0.45
P0_60_3	0	60	15.03	3.98	59.82	1001	1181	14.5	16.7	
P0_70_1	0	70	15.04	4.01	60.31	1182	1401	16.8	19.6	
P0_70_2	0	70	15.02	4.04	60.68	1237	1466	18.0	20.4	0.33
P0_70_3	0	70	15.03	4.04	60.72	1186	1428	16.8	19.5	
P0_80_1	0	80	15.12	4.03	60.93	1356	1671	20.4	22.3	
P0_80_2	0	80	15.09	4.05	61.11	1401	1720	20.7	22.9	0.24
P0_80_3	0	80	15.05	4.07	61.25	1372	1689	19.9	22.4	
P0_90_1	0	90	15.08	4.02	60.62	1577	2092	23.6	26.0	
P0_90_2	0	90	15.12	4.09	61.84	1618	2122	23.7	26.2	0.14
P0_90_3	0	90	15.07	4.09	61.64	1551	1992	22.7	25.2	
P30_10_1	30	10	15.10	4.01	60.55	527	750	8.5	8.7	
P30_10_2	30	10	15.09	4.05	61.11	538	739	8.5	8.8	10.72
P30_10_3	30	10	15.11	4.04	61.04	531	798	8.5	8.7	
P30_20_1	30	20	15.05	4.00	60.20	473	707	7.6	7.9	
P30_20_2	30	20	15.09	4.03	60.81	480	722	7.8	7.9	5.06
P30_20_3	30	20	15.10	4.01	60.55	480	722	7.8	7.9	
P30_30_1	30	30	15.08	4.06	61.22	599	766	9.1	9.8	
P30_30_2	30	30	15.02	4.01	60.23	596	761	9.2	9.9	1.39
P30_30_3	30	30	15.03	4.03	60.57	591	905	9.3	9.8	

P30_40_1	30	40	15.03	4.04	60.72	614	739	9.5	10.1	
P30_40_2	30	40	15.01	4.06	60.94	613	706	9.3	10.1	0.96
P30_40_3	30	40	15.00	4.04	60.60	618	764	9.6	10.2	
P30_50_1	30	50	15.10	3.99	60.25	860	1150	13.6	14.3	
P30_50_2	30	50	15.08	3.97	59.87	839	1135	13.3	14.0	0.66
P30_50_3	30	50	15.04	3.95	59.41	810	1109	13.2	13.6	
P30_60_1	30	60	15.04	4.02	60.46	980	1338	15.6	16.2	
P30_60_2	30	60	15.05	4.01	60.35	964	1325	15.2	16.0	0.41
P30_60_3	30	60	15.00	4.00	60.00	927	1304	14.9	15.5	
P30_70_1	30	70	15.01	4.03	60.49	1122	1599	17.8	18.5	
P30_70_2	30	70	15.05	4.03	60.65	1113	1561	17.6	18.4	0.29
P30_70_3	30	70	15.04	4.01	60.31	1116	1531	17.7	18.5	
P30_80_1	30	80	14.98	4.04	60.52	1132	1626	18.3	18.7	
P30_80_2	30	80	15.03	4.04	60.72	1190	1949	19.2	19.6	0.25
P30_80_3	30	80	14.96	4.03	60.29	1186	1739	19.2	19.7	
P30_90_1	30	90	15.09	4.04	60.96	1438	2164	22.8	23.6	
P30_90_2	30	90	15.00	4.02	60.30	1422	2201	22.9	23.6	0.11
P30_90_3	30	90	14.99	4.02	60.26	1384	2142	22.5	23.0	
P45_10_1	45	10	15.09	4.04	60.96	552	756	8.7	9.1	
P45_10_2	45	10	15.01	4.05	60.79	462	659	7.3	7.6	10.65
P45_10_3	45	10	14.95	4.05	60.55	492	693	8.0	8.1	
P45_20_1	45	20	15.06	4.09	61.60	661	935	10.7	10.7	
P45_20_2	45	20	14.93	4.14	61.81	548	896	8.5	8.9	5.12
P45_20_3	45	20	14.93	4.16	62.11	551	837	8.7	8.9	
P45_30_1	45	30	14.97	4.07	60.93	674	1011	10.9	11.1	
P45_30_2	45	30	14.94	4.16	62.15	661	989	10.4	10.6	1.37
P45_30_3	45	30	14.90	4.02	59.90	640	989	10.5	10.7	
P45_40_1	45	40	15.02	4.04	60.68	773	1130	12.7	12.7	
P45_40_2	45	40	15.03	4.01	60.27	747	1146	12.3	12.4	0.93
P45_40_3	45	40	14.90	4.07	60.64	730	1085	11.9	12.0	
P45_50_1	45	50	14.98	4.07	60.97	892	1323	14.6	14.6	
P45_50_2	45	50	14.98	4.01	60.07	856	1319	14.2	14.3	0.65
P45_50_3	45	50	15.00	4.00	60.00	807	1264	13.4	13.4	
P45_60_1	45	60	14.98	4.06	60.82	1008	1519	16.5	16.6	
P45_60_2	45	60	14.96	4.07	60.89	960	1448	15.7	15.8	0.43
P45_60_3	45	60	14.94	4.04	60.36	916	1383	15.1	15.2	
P45_70_1	45	70	14.89	4.07	60.60	1160	1713	19.0	19.1	
P45_70_2	45	70	14.99	4.12	61.76	1098	1643	17.6	17.8	0.31
P45_70_3	45	70	14.93	4.04	60.32	1055	1682	-	17.5	
P45_80_1	45	80	14.97	4.08	61.08	1269	1954	20.6	20.8	
P45_80_2	45	80	15.00	4.04	60.60	1243	1925	20.4	20.5	0.22
P45_80_3	45	80	14.99	4.01	60.11	1228	1920	20.2	20.3	

P45_90_1	45	90	14.99	4.03	60.41	1437	2224	23.5	23.8	
P45_90_2	45	90	14.96	4.08	61.04	1369	2162	22.3	22.4	0.13
P45_90_3	45	90	15.01	4.07	61.09	1356	2132	-	22.2	

Table 2 *(Continued on the next two pages)*. Summary of the experimental results generated by testing U-notched specimens.

Code	θ_P	In-fill	r_n	w_n	w_g	t	F_f	d_V
	[°]	*[%]*	*[mm]*	*[mm]*	*[mm]*	*[mm]*	*[N]*	*[mm]*
S0_30_1	0	30	0.50	15.23	24.94	4.14	730	
S0_30_2	0	30	0.51	15.29	24.79	4.11	533	1.42
S0_30_3	0	30	0.49	15.28	24.78	4.09	566	
S0_50_1	0	50	0.51	15.28	24.78	4.09	790	
S0_50_2	0	50	0.51	15.27	24.81	4.09	793	0.69
S0_50_3	0	50	0.48	15.28	24.81	4.15	879	
S0_70_1	0	70	0.53	15.31	24.78	4.16	1221	
S0_70_2	0	70	0.51	15.28	24.76	4.10	1023	0.33
S0_70_3	0	70	0.50	15.32	24.82	4.11	1046	
I0_30_1	0	30	1.01	15.31	24.73	4.03	504	
I0_30_2	0	30	1.03	15.31	24.72	4.04	545	1.45
I0_30_3	0	30	0.99	15.19	24.86	4.04	714	
I0_50_1	0	50	1.00	15.19	24.77	4.06	817	
I0_50_2	0	50	1.02	15.16	24.71	4.06	841	0.66
I0_50_3	0	50	1.00	15.21	24.75	4.05	884	
I0_70_1	0	70	1.01	15.27	24.81	4.08	1047	
I0_70_2	0	70	1.04	15.14	24.75	4.08	930	0.35
I0_70_3	0	70	1.00	15.08	24.75	4.04	1151	
B0_30_1	0	30	3.07	15.16	24.82	4.10	723	
B0_30_2	0	30	3.06	15.26	24.88	4.10	718	1.35
B0_30_3	0	30	3.04	15.29	24.82	4.12	599	
B0_50_1	0	50	3.04	15.19	24.86	4.15	893	
B0_50_2	0	50	3.06	15.29	24.97	4.12	871	0.67
B0_50_3	0	50	3.06	15.19	24.88	4.10	957	
B0_70_1	0	70	3.05	15.17	24.94	4.12	1222	
B0_70_2	0	70	3.06	15.20	24.94	4.12	1055	0.33
B0_70_3	0	70	3.08	15.14	24.82	4.07	1195	
S30_30_1	30	30	0.50	15.34	24.83	4.12	578	
S30_30_2	30	30	0.53	15.31	24.80	4.09	490	1.23
S30_30_3	30	30	0.51	15.34	24.77	4.04	470	
S30_50_1	30	50	0.51	15.32	24.86	4.15	810	0.68
S30_50_2	30	50	0.53	15.29	24.79	4.08	700	

S30_50_3	30	50	0.50	15.37	24.77	4.11	659	
S30_70_1	30	70	0.53	15.37	24.85	4.01	895	
S30_70_2	30	70	0.51	15.31	24.83	4.04	728	0.43
S30_70_3	30	70	0.51	15.32	24.78	4.07	640	
I30_30_1	30	30	1.01	15.16	24.72	4.03	503	
I30_30_2	30	30	1.03	15.17	24.74	4.04	539	1.44
I30_30_3	30	30	1.03	15.19	24.67	4.03	510	
I30_50_1	30	50	1.04	15.19	24.76	4.06	741	
I30_50_2	30	50	1.02	15.14	24.72	4.02	707	0.70
I30_50_3	30	50	1.01	15.24	24.76	4.04	768	
I30_70_1	30	70	1.02	15.11	24.72	4.00	739	
I30_70_2	30	70	1.03	15.19	24.77	4.04	718	0.39
I30_70_3	30	70	1.05	15.14	24.71	4.00	715	
B30_30_1	30	30	3.06	15.27	24.86	4.03	617	
B30_30_2	30	30	3.06	15.19	24.88	4.09	635	1.43
B30_30_3	30	30	3.07	15.20	24.85	4.06	608	
B30_50_1	30	50	3.07	15.25	24.82	4.05	797	
B30_50_2	30	50	3.07	15.07	24.86	4.08	767	0.72
B30_50_3	30	50	3.08	15.19	24.83	4.11	766	
B30_70_1	30	70	3.12	15.22	24.84	4.09	858	
B30_70_2	30	70	3.07	15.13	24.82	4.04	868	0.44
B30_70_3	30	70	3.09	15.16	24.98	4.06	848	
S45_30_1	45	30	0.50	15.37	24.81	4.01	450	
S45_30_2	45	30	0.55	15.29	24.75	3.99	443	1.19
S45_30_3	45	30	0.51	15.45	24.85	4.06	597	
S45_50_1	45	50	0.52	15.43	24.95	4.05	822	
S45_50_2	45	50	0.56	15.34	24.75	4.08	629	0.56
S45_50_3	45	50	0.54	15.32	24.82	4.02	604	
S45_70_1	45	70	0.54	15.40	24.85	4.03	909	
S45_70_2	45	70	0.55	15.29	24.75	4.00	841	0.36
S45_70_3	45	70	0.51	15.46	24.88	4.14	1070	
I45_30_1	45	30	1.04	15.25	24.74	4.01	536	
I45_30_2	45	30	1.06	15.22	24.66	3.96	502	1.42
I45_30_3	45	30	1.06	15.30	24.66	3.94	435	
I45_50_1	45	50	1.03	15.11	24.67	3.97	623	
I45_50_2	45	50	1.04	15.19	24.64	4.04	706	0.69
I45_50_3	45	50	1.04	15.19	24.76	4.00	839	
I45_70_1	45	70	1.05	15.11	24.75	4.01	949	
I45_70_2	45	70	1.06	15.14	24.66	3.96	964	0.38
I45_70_3	45	70	1.06	15.17	24.69	4.03	843	
B45_30_1	45	30	3.09	15.17	24.80	4.00	612	1.46
B45_30_2	45	30	3.08	15.12	24.89	4.03	596	

B45_30_3	45	30	3.25	15.26	25.05	4.02	592	
B45_50_1	45	50	3.06	15.14	24.89	4.04	854	
B45_50_2	45	50	3.08	15.17	24.87	4.06	836	0.69
B45_50_3	45	50	3.09	15.19	24.87	4.07	794	
B45_70_1	45	70	3.08	15.17	24.82	4.08	998	
B45_70_2	45	70	3.08	15.16	25.02	4.08	1058	0.38
B45_70_3	45	70	3.06	15.09	24.88	4.08	977	

Table 3 *(Continued on the next two pages)*. Summary of the experimental results generated by testing specimens containing open notches.

Code	**θ_P**	**In-fill**	**r_n**	**w_n**	**w_g**	**t**	**F_f**	**d_V**
	[°]	*[%]*	*[mm]*	*[mm]*	*[mm]*	*[mm]*	*[N]*	*[mm]*
OS0_30_1	0	30	0.55	15.20	24.73	3.96	381	
OS0_30_2	0	30	0.56	15.14	24.73	3.95	419	1.54
OS0_30_3	0	30	0.55	15.20	24.65	3.98	396	
OS0_50_1	0	50	0.53	15.09	24.61	4.02	706	
OS0_50_2	0	50	0.53	15.15	24.64	4.06	664	0.66
OS0_50_3	0	50	0.54	15.09	24.69	4.04	631	
OS0_70_1	0	70	0.49	15.16	24.67	4.00	909	
OS0_70_2	0	70	0.54	15.17	24.66	3.99	860	0.33
OS0_70_3	0	70	0.61	15.18	24.68	4.02	860	
OI0_30_1	0	30	1.04	15.12	24.82	4.02	522	
OI0_30_2	0	30	1.07	15.20	24.69	3.98	518	1.45
OI0_30_3	0	30	1.14	15.19	24.74	3.94	509	
OI0_50_1	0	50	1.06	15.19	24.92	4.04	712	
OI0_50_2	0	50	0.97	15.21	24.91	4.05	730	0.65
OI0_50_3	0	50	1.07	15.23	24.77	4.03	706	
OI0_70_1	0	70	1.05	15.16	24.73	4.06	977	
OI0_70_2	0	70	1.05	15.17	24.78	4.04	999	0.35
OI0_70_3	0	70	0.99	15.13	24.76	4.00	1044	
OB0_30_1	0	30	2.89	15.22	25.08	3.95	499	
OB0_30_2	0	30	2.80	15.06	24.87	3.97	493	1.44
OB0_30_3	0	30	3.03	14.98	24.76	4.01	508	
OB0_50_1	0	50	3.01	15.00	24.87	3.93	672	
OB0_50_2	0	50	2.99	14.99	24.82	3.93	657	0.67
OB0_50_3	0	50	3.05	14.98	24.80	4.00	658	
OB0_70_1	0	70	2.94	15.14	24.87	4.00	921	
OB0_70_2	0	70	3.08	15.03	24.76	4.04	919	0.37
OB0_70_3	0	70	3.04	15.05	24.80	4.07	929	
OS30_30_1	30	30	0.55	15.29	24.65	4.02	420	1.56

OS30_30_2	30	30	0.62	15.25	24.63	4.03	412	
OS30_30_3	30	30	0.59	15.26	24.61	4.01	461	
OS30_50_1	30	50	0.50	15.33	24.89	4.07	1056	
OS30_50_2	30	50	0.50	15.27	24.85	4.08	944	0.65
OS30_50_3	30	50	0.49	15.30	24.81	4.11	1065	
OS30_70_1	30	70	0.54	15.03	24.63	4.01	861	
OS30_70_2	30	70	0.53	15.12	24.80	3.99	807	0.40
OS30_70_3	30	70	0.55	15.24	24.77	4.00	790	
OI30_30_1	30	30	1.02	15.25	24.85	4.04	554	
OI30_30_2	30	30	0.95	15.22	24.87	3.97	588	1.56
OI30_30_3	30	30	0.99	15.41	24.81	4.02	557	
OI30_50_1	30	50	1.03	15.38	24.84	4.11	1100	
OI30_50_2	30	50	0.97	15.33	24.79	4.09	1055	0.65
OI30_50_3	30	50	1.04	15.29	24.87	4.08	1088	
OI30_70_1	30	70	1.02	15.22	24.83	4.02	961	
OI30_70_2	30	70	1.02	15.05	24.75	4.05	923	0.38
OI30_70_3	30	70	1.07	15.32	24.75	4.01	997	
OB30_30_1	30	30	2.97	15.05	24.67	4.03	458	
OB30_30_2	30	30	2.98	15.00	24.82	4.00	452	1.50
OB30_30_3	30	30	3.06	15.03	24.89	4.06	510	
OB30_50_1	30	50	2.96	15.02	24.72	4.06	1005	
OB30_50_2	30	50	3.02	15.05	24.63	4.05	1009	0.68
OB30_50_3	30	50	2.96	15.07	24.75	4.09	1075	
OB30_70_1	30	70	3.04	15.10	24.88	4.09	858	
OB30_70_2	30	70	2.98	14.93	24.70	4.03	783	0.36
OB30_70_3	30	70	3.06	15.07	24.68	4.00	779	
OS45_30_1	45	30	0.42	15.40	24.74	4.05	724	
OS45_30_2	45	30	0.52	15.53	24.75	4.05	795	1.52
OS45_30_3	45	30	0.47	15.65	24.73	4.08	726	
OS45_50_1	45	50	0.51	15.50	24.74	4.01	1013	
OS45_50_2	45	50	0.52	15.27	24.76	4.01	1064	0.7
OS45_50_3	45	50	0.50	15.60	24.78	4.05	1065	
OS45_70_1	45	70	0.49	15.42	24.74	4.08	1333	
OS45_70_2	45	70	0.49	15.56	25.22	4.02	1283	0.32
OS45_70_3	45	70	0.52	15.34	24.76	4.03	1235	
OI45_30_1	45	30	1.04	15.45	24.80	4.04	815	
OI45_30_2	45	30	1.12	15.52	24.79	4.09	815	1.45
OI45_30_3	45	30	1.01	15.59	24.85	4.05	780	
OI45_50_1	45	50	1.07	15.52	24.86	4.04	1086	
OI45_50_2	45	50	0.99	15.31	24.90	4.06	537	0.69
OI45_50_3	45	50	1.03	15.37	24.82	4.06	1038	
OI45_70_1	45	70	1.07	15.37	24.84	4.07	1353	0.31

OI45_70_2	45	70	1.10	15.18	24.88	4.08	1323	
OI45_70_3	45	70	1.03	15.13	24.94	4.11	1295	
OB45_30_1	45	30	3.03	15.06	24.84	4.06	732	
OB45_30_2	45	30	3.01	15.00	24.84	4.05	789	1.49
OB45_30_3	45	30	3.02	15.19	24.98	4.08	801	
OB45_50_1	45	50	2.94	15.06	24.85	4.01	1026	
OB45_50_2	45	50	2.87	15.05	24.81	4.03	1024	0.70
OB45_50_3	45	50	2.89	15.10	24.90	4.05	1094	
OB45_70_1	45	70	3.07	15.07	24.80	4.04	1256	
OB45_70_2	45	70	3.00	15.05	24.80	4.06	1215	0.32
OB45_70_3	45	70	2.89	15.02	24.77	4.02	1220	

Figures

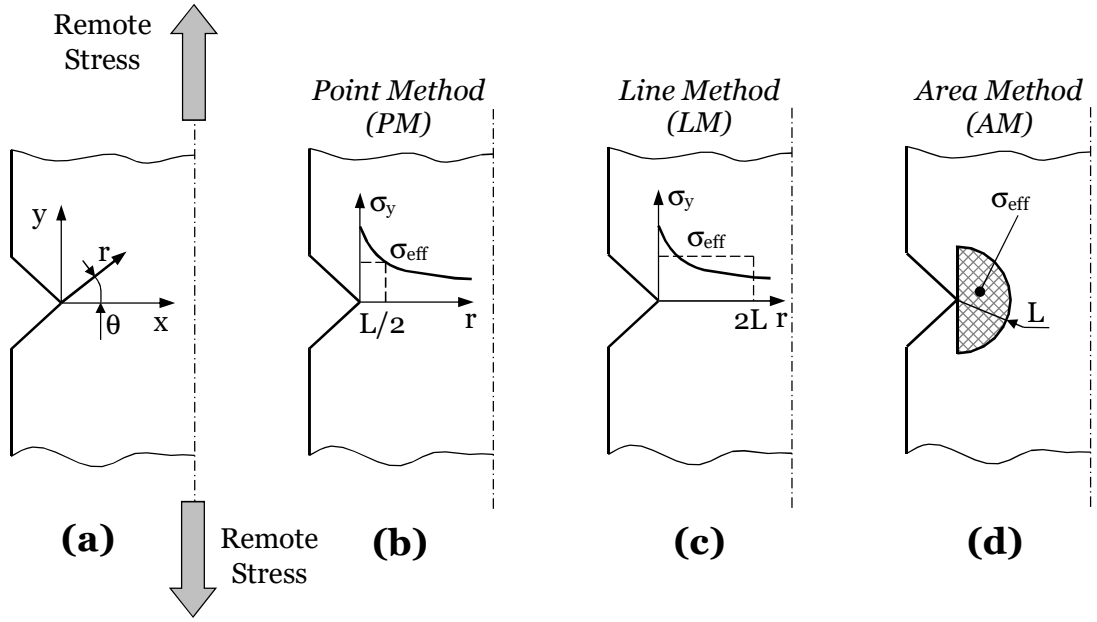

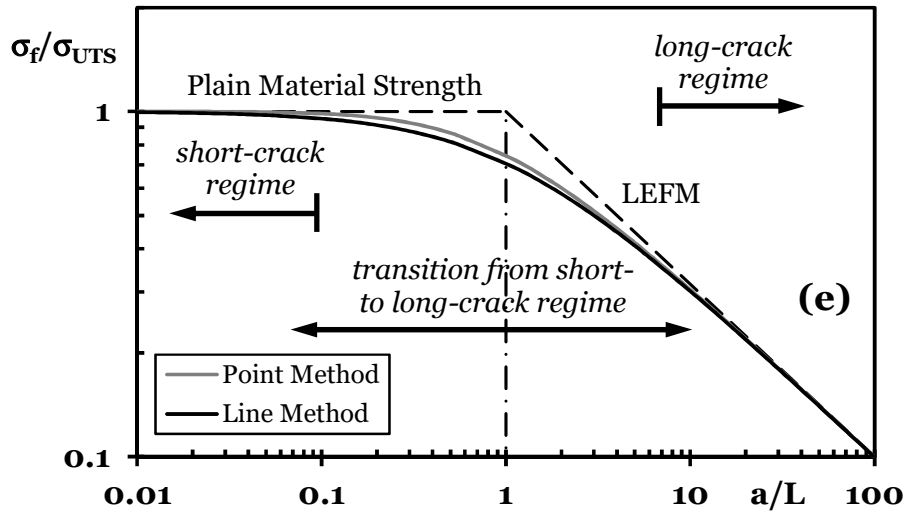

Figure 1. Notch/crack loaded in tension (a); the TCD formalised according to the PM (b), the LM (c) and the AM (d); modelling the transition from the short- to the long-crack regime according to the TCD (e).

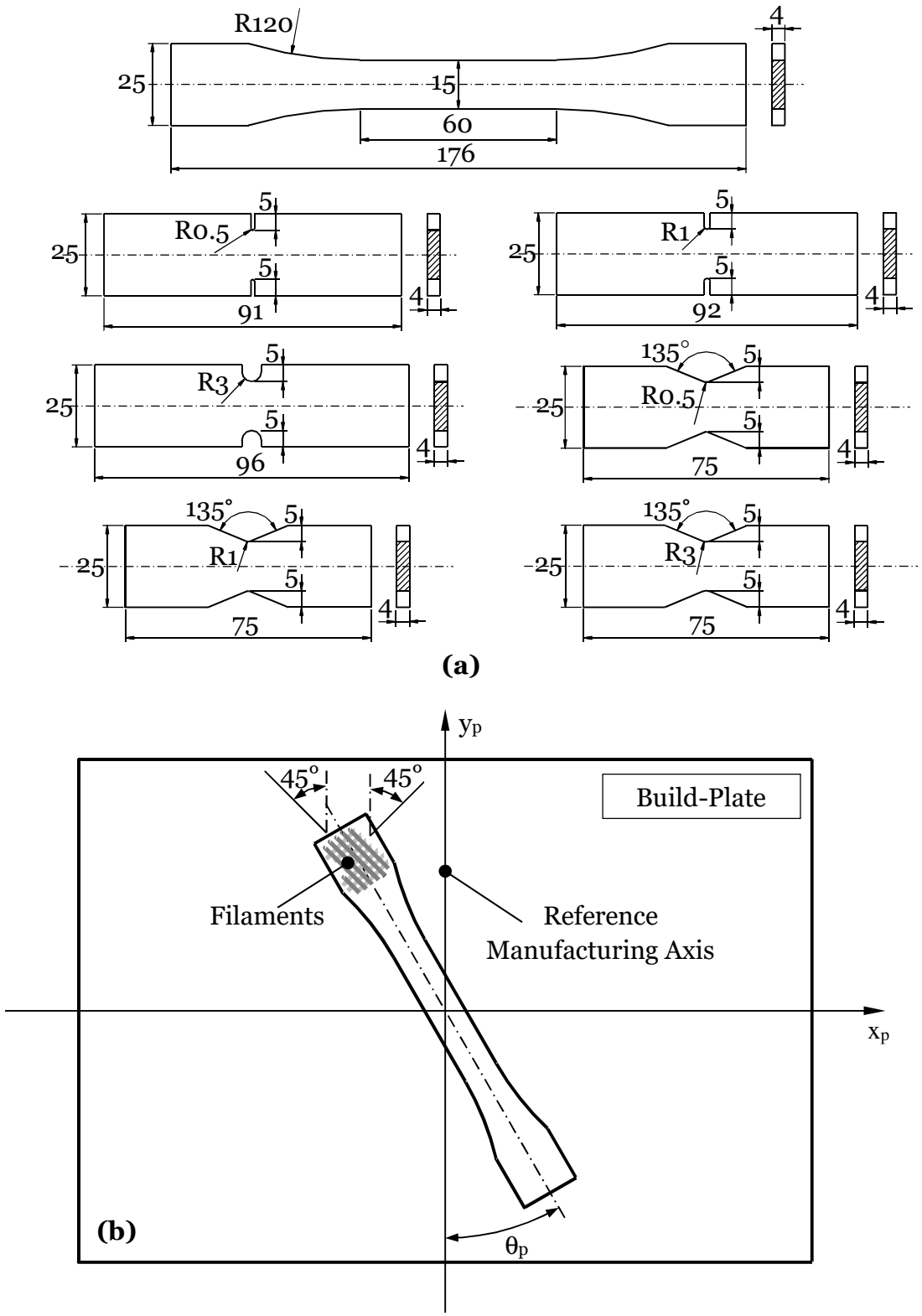

Figure 2. Technical drawings showing the geometries of the AM specimens being tested (a) – dimensions in millimetres; manufacturing angle θ_p and orientation of the deposition filaments (b).

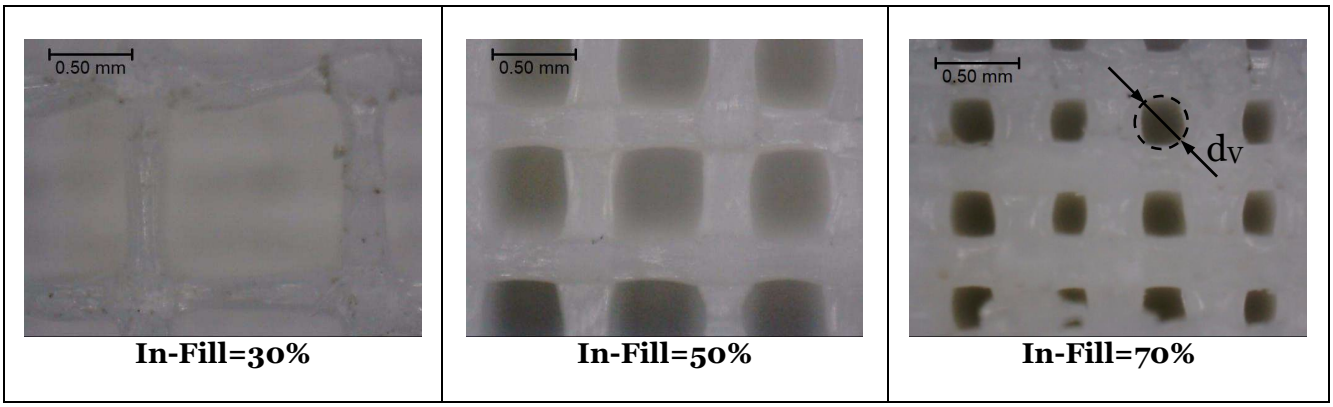

Figure 3. Examples of: (a) honeycomb-like structure obtained by setting the fill density equal to 30%, 50%, and 70%; (b) cracking behaviour observed for different values of manufacturing angle θ_p and different in-fill levels (the specimens' longitudinal axis is vertical).

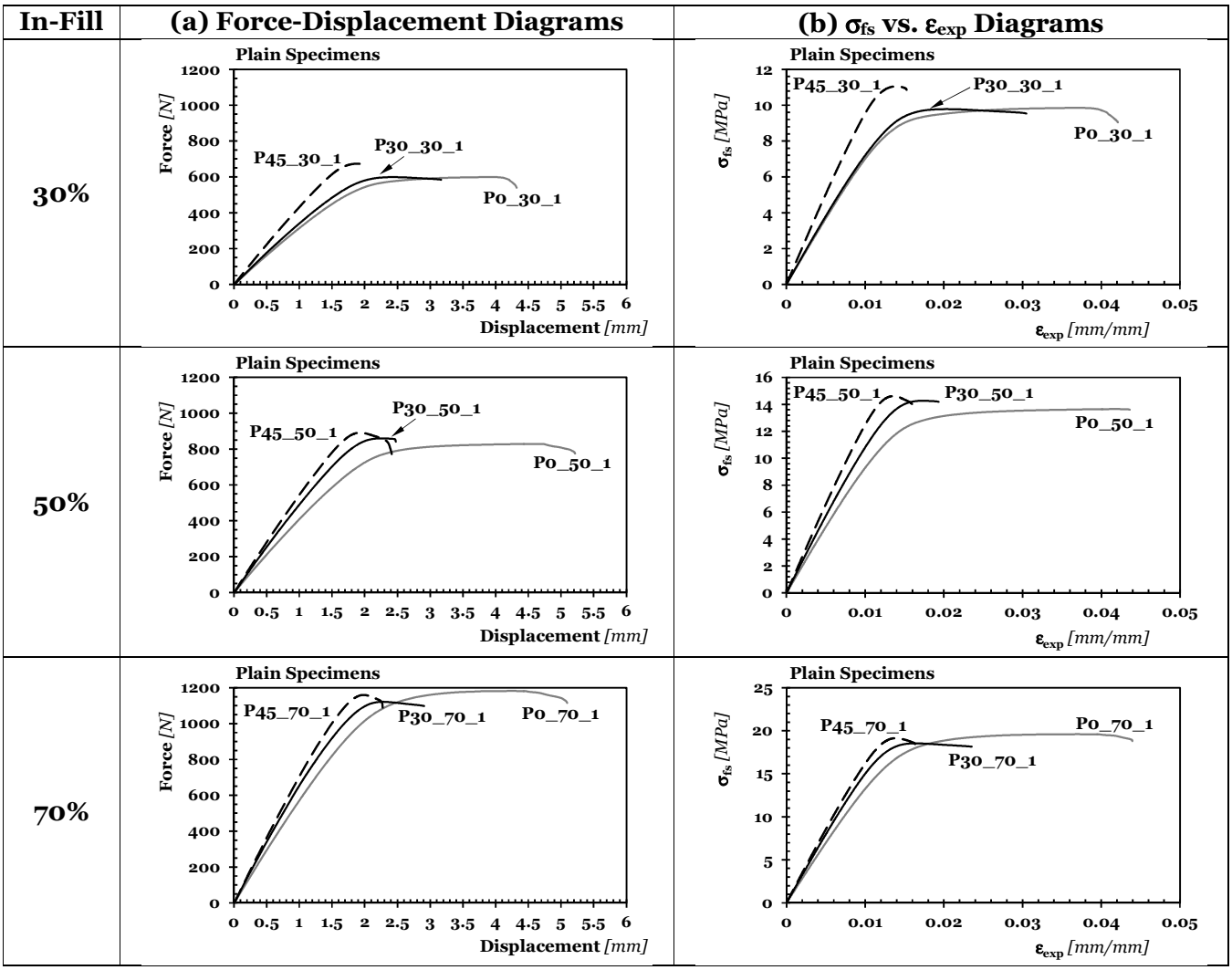

Figure 4. Examples of force vs. displacement behaviour displayed by the plain specimens (a) and corresponding fictitious stress, σ_{fs}, vs. experimental strain, ε_{exp}, diagrams (b).

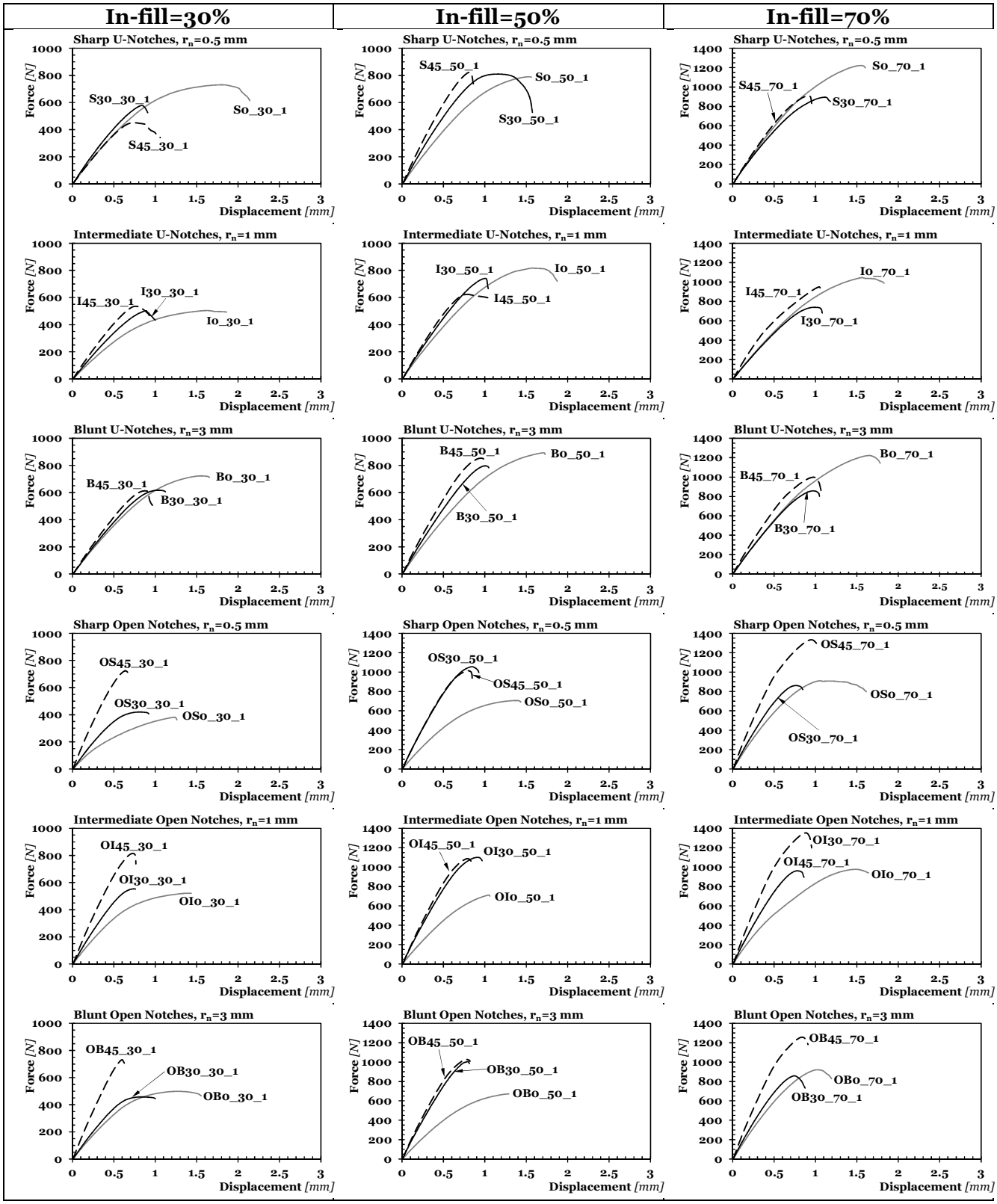

Figure 5. Examples of force vs. displacement behaviour displayed by the notched specimens being tested.

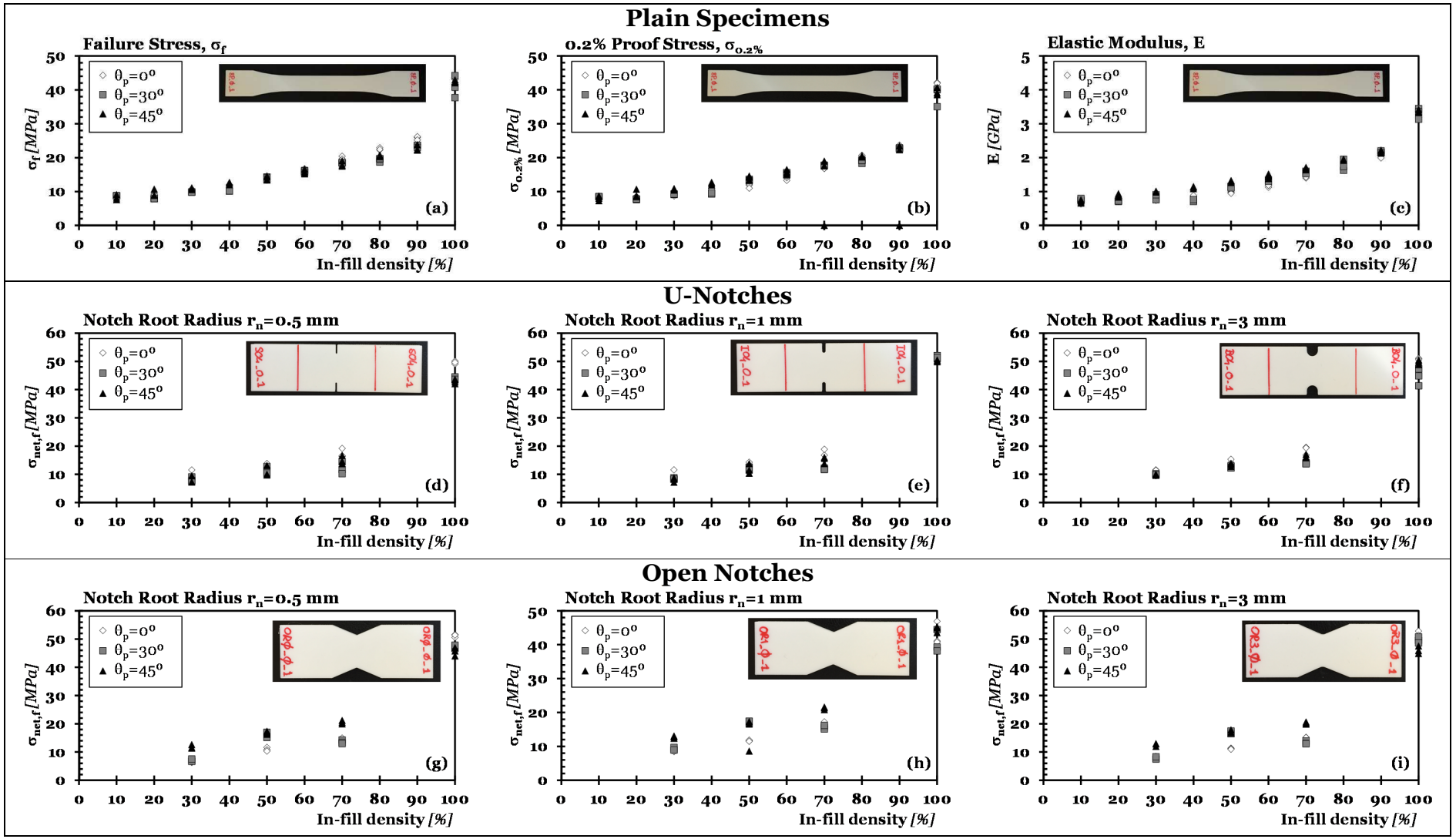

Figure 6. Mechanical properties (a to c) and notch strength (d to i) of the AM PLA being tested for different in-fill levels – the results for a fill density equal to 100% are taken from Ref. [6].

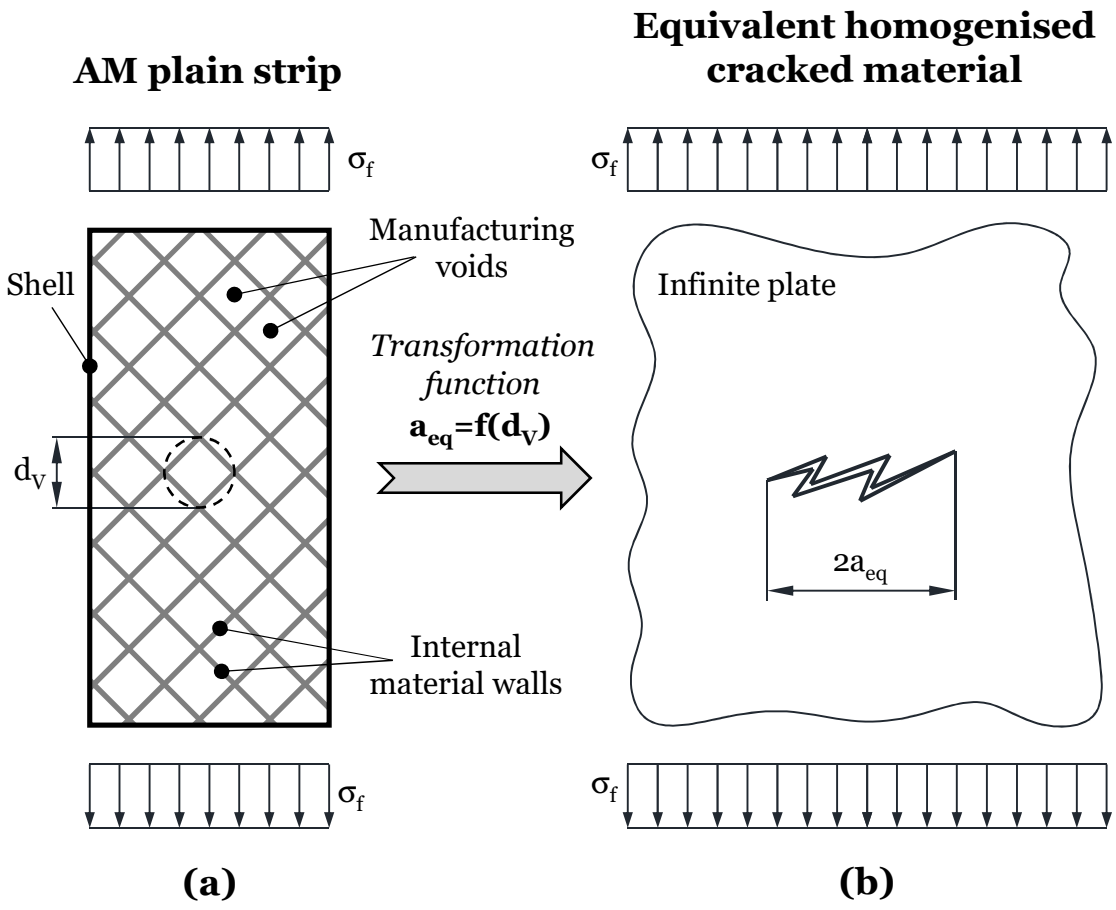

Figure 7. Transformation process to estimate static strength of plain PLA additively manufactured with different in-fill levels.

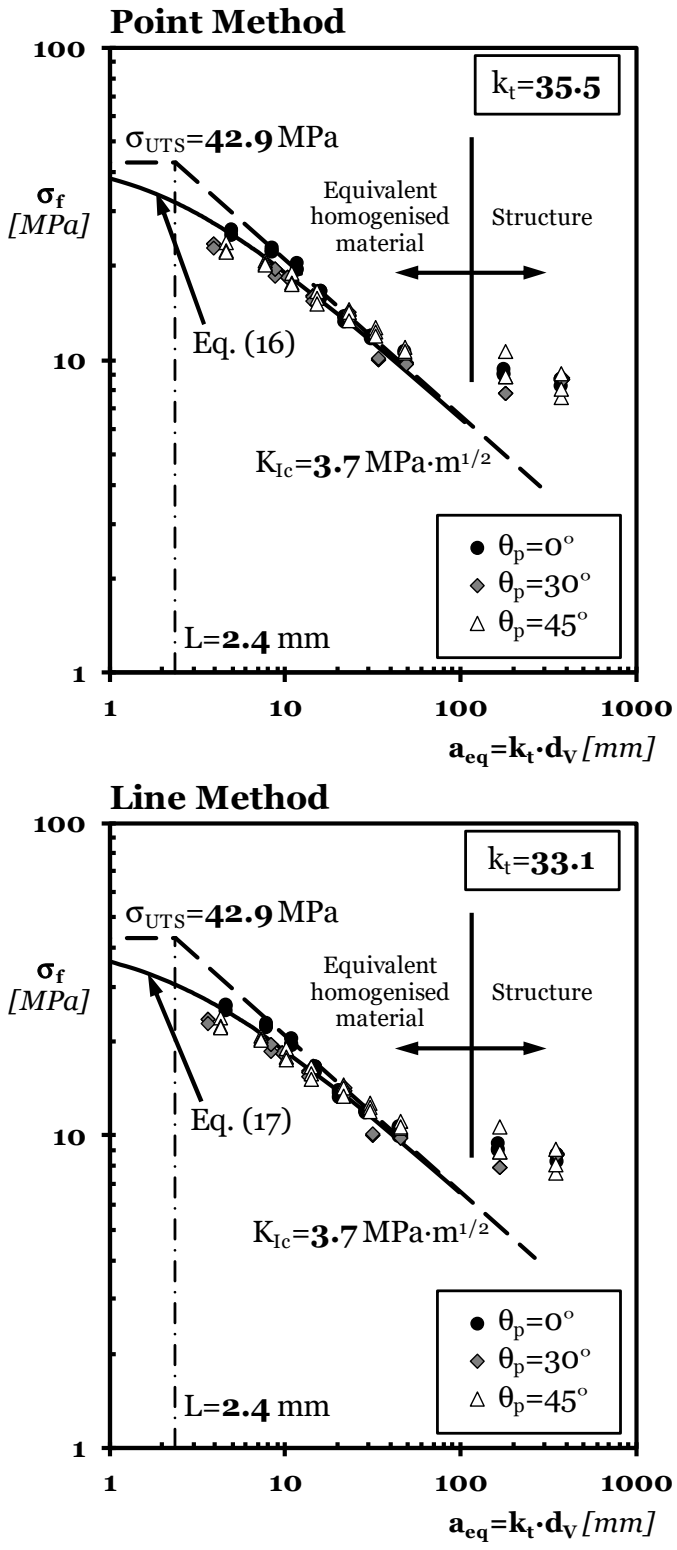

Figure 8. Accuracy of the proposed methodology in modelling plain static strength of PLA additively manufactured with different in-fill levels.

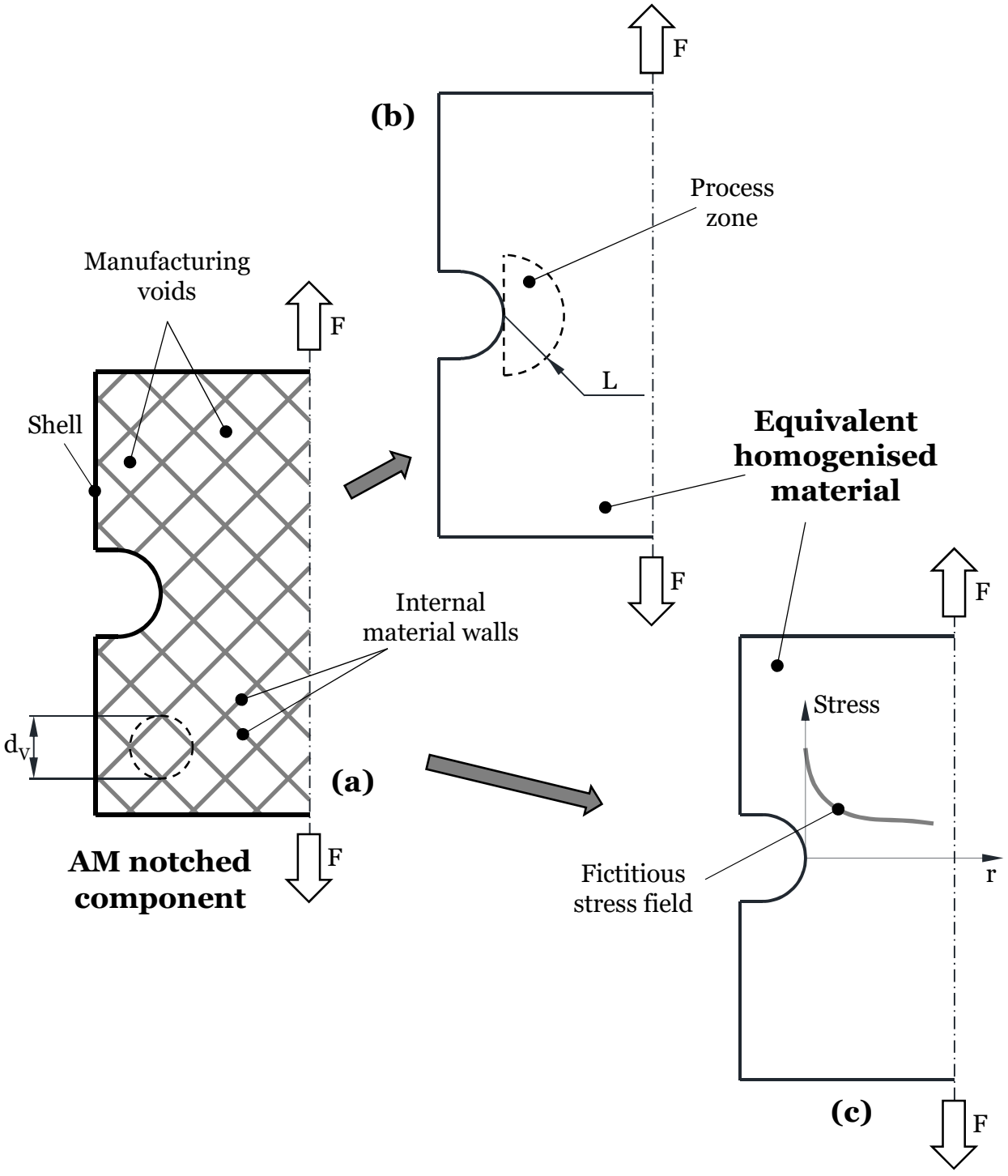

Figure 9. Process zone and fictitious linear-elastic local stress fields to perform static assessment of notched objects of AM PLA.

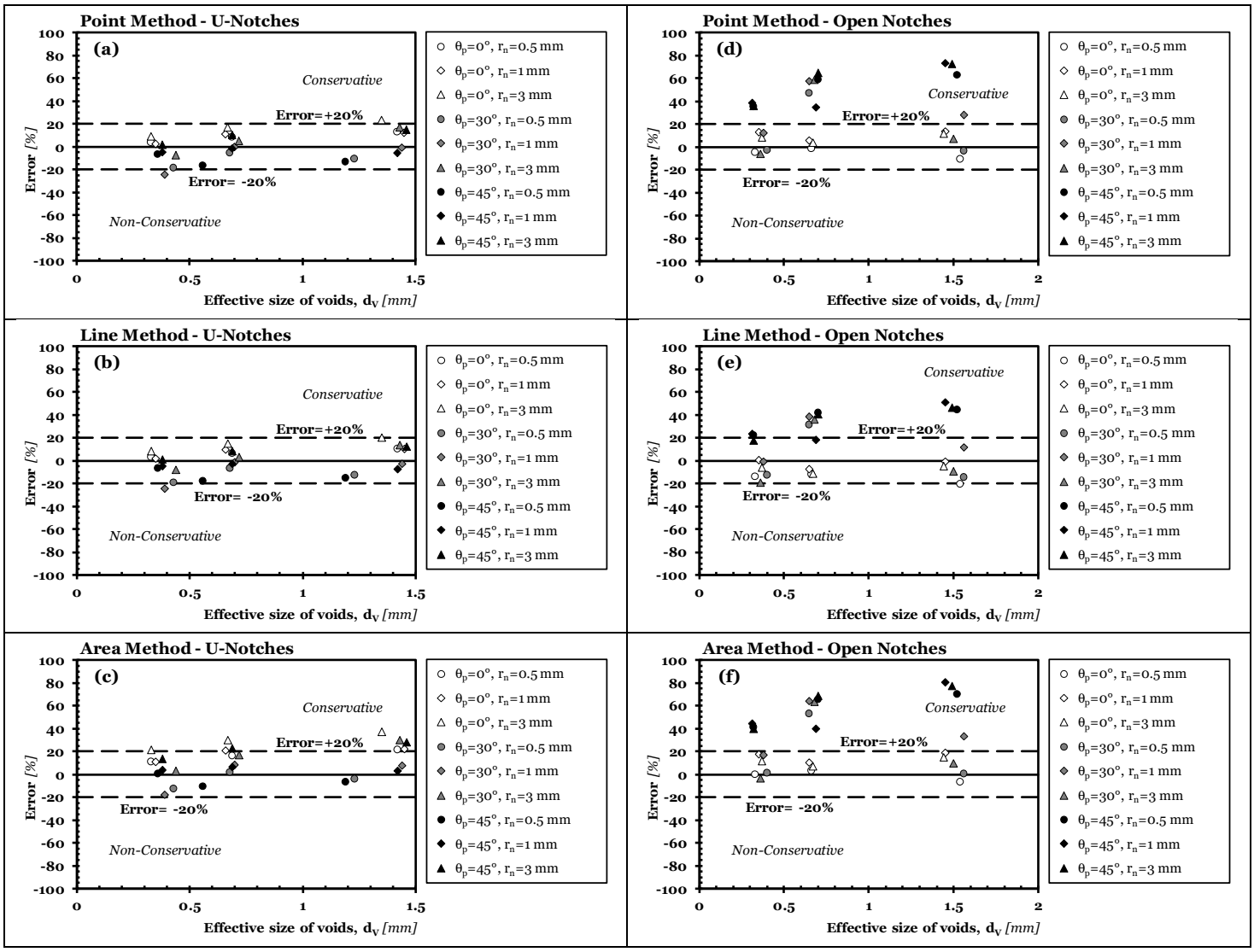

Figure 10. Accuracy of the TCD applied along with the equivalent homogenised material concept in estimating the static strength of the notched specimens of AM PLA being tested.